Biological pattern formation: from basic mechanisms to complex structures

A. J. Koch* and H. Meinhardt

Max-Planck-Institut für Entwicklungsbiologie, Spemannstrasse 35/IV, D-72076 Tübingen, Germany

The reliable development of highly complex organisms is an intriguing and fascinating problem. The genetic material is, as a rule, the same in each cell of an organism. How then do cells, under the influence of their common genes, produce spatial patterns? Simple models are discussed that describe the generation of patterns out of an initially nearly homogeneous state. They are based on nonlinear interactions of at least two chemicals and on their diffusion. The concepts of local autocatalysis and of long-range inhibition play a fundamental role. Numerical simulations show that the models account for many basic biological observations such as the regeneration of a pattern after excision of tissue or the production of regular (or nearly regular) arrays of organs during (or after) completion of growth. Very complex patterns can be generated in a reproducible way by hierarchical coupling of several such elementary reactions. Applications to animal coats and to the generation of polygonally shaped patterns are provided. It is further shown how to generate a strictly periodic pattern of units that themselves exhibit a complex and polar fine structure. This is illustrated by two examples: the assembly of photoreceptor cells in the eye of *Drosophila* and the positioning of leaves and axillary buds in a growing shoot. In both cases, the substructures have to achieve an internal polarity under the influence of some primary pattern-forming system existing in the fly's eye or in the plant. The fact that similar models can describe essential steps in organisms as distantly related as animals and plants suggests that they reveal some universal mechanisms.

CONTENTS

I. INTRODUCTION

A most fascinating aspect of biological systems is the generation of complex organisms in each round of the life cycle. Higher organisms develop, as the rule, from a single fertilized egg. The result is a highly reproducible arrangement of differentiated cells. Many processes are involved, for example, cell differentiation, cell movement, shape changes of cells and tissues, region-specific control of cell division, and cell death. Development of an organism is, of course, under genetic control, but the genetic information is usually the same in all cells. A crucial problem is therefore the generation of spatial patterns that allow a different fate for some cells than for others.

The complexity of the evolving pattern seems to preclude any mathematical theory. However, by experimental interference with a developing organism it has turned out that the individual steps are fairly independent of each other. For instance, the organization of the anteroposterior axis (i.e., the head-to-tail pattern) in a *Drosophila* embryo is controlled by a completely different set of genes than the dorsoventral axis. Shortly after its initiation, the development of a wing is largely independent of the surrounding tissue and can progress even in an ectopic position after transplantation. Therefore models can be written for elementary steps in development. The linkage of these steps then requires a second approximation.

The necessity of mathematical models for morphogenesis is evident. Pattern formation is certainly based on the interaction of many components. Since the interactions are expected to be nonlinear, our intuition is insufficient to check whether a particular assumption really accounts for the experimental observation. By modeling, the weak points of an hypothesis become evident and the initial hypothesis can be modified or improved. Models often contain simplifying assumptions, and different models may account equally well for a particular observation. This diversity should, however, be considered as an advantage: multiplicity of models stimulates the design of experimental tests in order to discriminate between the

*Present address: Institut de Physique Expérimentale, Université de Lausanne, CH-1015 Lausanne, Switzerland.

 0034-6861/94/66(4)/1481(27)/$07.70

rival theories. In this way, theoretical considerations provide substantial help in understanding the mechanisms on which development is based (Berking, 1981).

In his pioneering work, Turing (1952) has shown that under certain conditions two interacting chemicals can generate a stable inhomogeneous pattern if one of the substances diffuses much faster than the other. This result goes against "common sense," since diffusion is expected to smooth out concentration differences rather than to generate them.

Turing apologizes for the strange and unlikely chemical reaction he used in his study. Since then, biochemically more feasible models have been developed and applied to different developmental situations (Lefever, 1968; Gierer and Meinhardt, 1972; Gierer, 1977; Murray, 1990). Chemical systems have also been intensively investigated for their ability to produce "Turing patterns": some experiments present beautiful reaction-diffusion structures in open reactors (Ouyang *et al.*, 1989; Castets *et al.*, 1990; de Kepper *et al.*, 1991).

In the first part of this article, after briefly discussing the relevance of chemical gradients in biological systems, we shall present simple models of pattern formation and their common basis, *local self-enhancement* and *long-range inhibition.* The patterns that can be generated are graded concentration profiles, local concentration maxima, and stripelike distributions of substances. In the second part we shall show how more complex patterns can be generated by hierarchical superimposition of several pattern-forming systems. The formation of a regular periodic arrangement of different cell types or the generation of polygonal patterns will be discussed. The models of that section are original and up until now unpublished.

Appendix A contains a complete discussion of linear stability analysis in the case of the simplest models. The parameters used for the simulations presented hereafter are listed in Appendix B. A reader interested in numerical simulations should have no difficulty in reproducing or improving upon the results.

Throughout the paper, comparisons of models with experimental observations are provided. If necessary, the biological background is outlined in such a way that the article should be understandable without previous knowledge of biology.

II. GRADIENTS IN BIOLOGICAL SYSTEMS

In many developmental systems small regions play an important role because they are able to organize the fate of the surrounding tissue. The mouth opening of a hydra or the dorsal lip of an amphibian blastula are well-known examples. Transplantation of a small piece of such an organizing center into an ectopic position can change the fate of the surrounding tissue: these cells are then instructed to form those structures that are induced in the normal neighborhood of such an organizing region. Based on these observations, Wolpert (1969) has worked out the concept of positional information. The local concentration of a substance that is distributed in a graded fashion dictates the direction in which a group of cells has to develop. The organizing region is thought to be the source of such a morphogenetic substance. A famous example is the determination of the digits in the chick wing bud (Cooke and Summerbell, 1980; Tickle, 1981). It occurs under control of a small nest of cells located at the posterior border of the wing bud, the zone of polarizing activity (ZPA). The results fit nicely with the assumption of some hypothetical substance diffusing out of the ZPA and producing a concentration gradient; groups of cells form the correct digit by measuring the local concentration within this gradient (Summerbell, 1974; Wolpert and Hornbruch, 1981). Many experiments in which a second ZPA is implanted at various positions of the wing bud confirm this conjecture: supernumerary digits are then formed at abnormal positions but in accordance with the pattern predicted by the assumed gradient produced by the two ZPA. A possible candidate for the morphogenetic substance is retinoic acid (Thaller and Eichele, 1987, 1988). Indeed, small beets soaked with this substance at low concentrations mimic all the effects of a ZPA.

Today there is a growing body of evidence that chemical gradients play a key role in pattern formation and cell differentiation. For instance, it has been observed that the protein *bicoid* has a graded concentration distribution in the *Drosophila melanogaster* embryo; it organizes the anterior half of the fly and has been fully characterized (Driever and Nüsslein-Volhard, 1988; Boring *et al.*, 1993).

In this context, theoretical models have to give satisfactory answers to the following two questions:

(i) How can a system give rise to and maintain large-scale inhomogeneities like gradients even when starting from initially more or less homogeneous conditions?

(ii) How do cells measure the local concentration in order to interpret their position in a gradient and choose the corresponding developmental pathway?

The next two sections are devoted to the first question. We shall discuss theoretical models having the ability to produce graded distributions of chemical substances and present their regulation characteristics. In the subsequent section, we shall show how to use the positional information contained in gradients in order to induce a correct differentiation.

III. SIMPLE MODELS FOR PATTERN FORMATION

As mentioned, Turing (1952) was the first to realize that the interaction of two substances with different diffusion rates can cause pattern formation. Gierer and Meinhardt (1972) and independently Segel and Jackson (1972) have shown that two features play a central role: *local self-enhancement* and *long-range inhibition.* It is essential to have an intuitive understanding of these two requirements, since they lie at the heart of pattern formation.

Self-enhancement is essential for small local inhomogeneities to be amplified. A substance a is said to be *self-enhancing* or *autocatalytic* if a small increase of a over its homogeneous steady-state concentration induces a further increase of a.[1] The self-enhancement does not need to be direct: a substance a may promote the production rate of a substance b and vice versa; or, as will be discussed further below, two chemicals that mutually inhibit each other's production may act together like an autocatalytic substance.

Self-enhancement alone is not sufficient to generate stable patterns. Once a begins to increase at a given position, its positive feedback would lead to an overall activation. Thus the self-enhancement of a has to be complemented by the action of a fast-diffusing antagonist. The latter prevents the spread of the self-enhancing reaction into the surrounding tissue without choking the incipient local increase. Two types of antagonistic reactions are conceivable. Either an inhibitory substance h is produced by the activator that, in turn, slows down the activator production or a substrate s is consumed during autocatalysis. Its depletion slows down the self-enhancing reaction.

A. Activator-inhibitor systems

The following set of differential equations describes a possible interaction between an activator a and its rapidly diffusing antagonist h (Gierer and Meinhardt, 1972):

$$\frac{\partial a}{\partial t} = D_a \triangle a + \rho_a \frac{a^2}{(1+\kappa_a a^2)h} - \mu_a a + \sigma_a \ , \qquad (1a)$$

$$\frac{\partial h}{\partial t} = D_h \triangle h + \rho_h a^2 - \mu_h h + \sigma_h \ , \qquad (1b)$$

where $\triangle$ is the Laplace operator; in a two-dimensional orthonormal coordinate system, $\triangle = \partial^2/\partial x^2 + \partial^2/\partial y^2$. D_a, D_h are the diffusion constants, μ_a, μ_h the removal rates, and ρ_a, ρ_h the cross-reaction coefficients; σ_a, σ_h are basic production terms; κ_a is a saturation constant.

As discussed above, lateral inhibition of a by h requires that the antagonist h diffuse faster than the self-enhanced substance a: $D_h \gg D_a$.[2] This is not yet sufficient to generate stable patterns. We show in Appendix A that in addition the inhibitor has to adapt rapidly to any change of the activator. This is the case if the removal rate of h is large compared to that of a: $\mu_h > \mu_a$. Otherwise the system oscillates or produces traveling waves.

Though not necessary for pattern formation, the saturation constant κ_a has a deep impact on the final aspect of the pattern. Without saturation, somewhat irregularly arranged peaks are formed whereby a maximum and minimum distance between the maxima is maintained [Figs. 1(a) and 1(b)]. In contrast, if the autocatalysis saturates ($\kappa_a > 0$), the inhibitor production is also limited. A stripelike pattern emerges. In this arrangement activated cells have activated neighbors; nevertheless nonactivated areas are close by into which the inhibitor can diffuse [Fig. 1(c)].

Embryonic development often makes use of stripe formation. For example, genes essential for the segmentation of insects are activated in narrow stripes that surround the embryo in a beltlike manner (Ingham, 1991). In monkeys, the nerves of the right and the left eye project onto adjacent stripes in the cortex (Hubel *et al.*, 1977). The stripes of a zebra are proverbial.

By convenient choice of the concentration units for a and h, it is always possible to set $\mu_a = \rho_a$ and $\mu_h = \rho_h$ (Appendix A). Moreover, some constants involved in Eq. (1) are not essential for the morphogenetic ability of this system (they are useful if one needs "fine tuning" of the regulation properties). In its simplest form, the activator-inhibitor model is written:

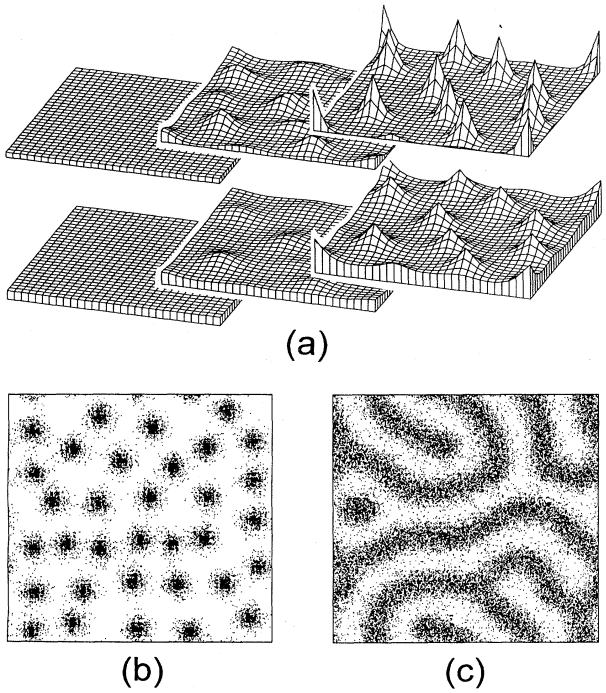

FIG. 1. Patterns produced by the activator-inhibitor model (1): (a) Initial, intermediate, and final activator (top) and inhibitor (bottom) distribution. (b) Result of a similar simulation in a larger field. The concentration of the activator is suggested by the dot density. (c) Saturation of autocatalysis ($\kappa_a > 0$) can lead to a stripelike arrangement of activated cells.

[1]To simplify the notations, we shall use the same symbol to designate a chemical species and its concentration. This should not lead to any confusion.

[2]Here are some orders of magnitude for the diffusion constants in cells. Roughly speaking, the diffusion constants in cytoplasm range from 10^{-6} $cm^2\,s^{-1}$ for small molecules to 10^{-8} $cm^2\,s^{-1}$ for proteins. Diffusion from cell to cell via gap junctions lowers these values by a factor of 10 (Crick, 1970; Slack, 1987).

$$\frac{\partial a}{\partial t} = D_a \triangle a + \rho_a \left(\frac{a^2}{h} - a \right) , \tag{2a}$$

$$\frac{\partial h}{\partial t} = D_h \triangle h + \rho_h \left(a^2 - h \right) . \tag{2b}$$

Convenient length and time units can be found in which $\rho_a = D_h = 1$. This reduces the number of essential parameters to two, namely, D_a and ρ_h.

B. Activator-substrate systems

Lateral inhibition can also be achieved by the depletion of a substance s required for the autocatalysis:

$$\frac{\partial a}{\partial t} = D_a \triangle a + \rho_a \frac{a^2 s}{1 + \kappa_a a^2} - \mu_a a + \sigma_a , \tag{3a}$$

$$\frac{\partial s}{\partial t} = D_s \triangle s - \rho_s \frac{a^2 s}{1 + \kappa_a a^2} + \sigma_s . \tag{3b}$$

The parameters D_a, D_s, μ_a, ρ_a, ρ_s, κ_a, σ_a, and σ_s have the same meaning as in Eq. (1); a is the self-enhanced reactant, while s plays the role of the antagonist and can be interpreted as a *substrate* depleted by a. For this reason, we shall refer to this system as the *activator-substrate model.* Lateral inhibition of a by s is effective if $D_s \gg D_a$. The model has similarities to the well-known Brusselator (Lefever, 1968; Auchmuty and Nicolis, 1975; Vardasca *et al.*, 1992).

Suitable concentration units for a and s allow us to set $\mu_a = \rho_a$ and $\sigma_s = \rho_s$. In its simplest form, the system looks like

$$\frac{\partial a}{\partial t} = D_a \triangle a + \rho_a \left(a^2 s - a \right) , \tag{4a}$$

$$\frac{\partial s}{\partial t} = D_s \triangle s + \rho_s \left(1 - a^2 s \right) . \tag{4b}$$

One can always adapt the time and length units so that $\rho_a = D_s = 1$; only two parameters, ρ_s and D_a, then remain.

Figure 2 presents typical patterns resulting from such a model. The activator-substrate (a, s) and activator-inhibitor (a, h) models have some distinctly different properties. As can be seen in Fig. 2, in (a, s) systems the activator forms rounded mounds, in contrast to sharp peaks of (a, h) models [Fig. 1(a)]. In a growing field of cells, an (a, s) system produces new maxima preferentially by a split and shift of existing ones, while in (a, h) models new peaks are inserted at the maximum distance from the existing ones. The reason for the shift of maxima in an (a, s) system is the following. With growth, the substrate concentration increases in the enlarging space between the activated regions. This can lead to a higher activator production at the side of a maximum if compared with its center. In such a case the maximum begins to wander towards higher substrate concentrations until a new optimum is reached. In (a, h) systems, a maximum suppresses more efficiently the formation of other maxima in the surroundings. This is evident from Figs. 1 and 2. In the former case the distance between the maxima is much higher, although corresponding parameters have been used for both simulations (see Appendix B). We shall often make use of these different properties. If a maximum has to be displaced or to form a wave, one will preferentially use an (a, s) system. In contrast, if an isolated maximum has to be generated, we shall employ an (a, h) system. The ultimate reason for this different behavior is the inherent saturation in the (a, s) system. The autocatalysis must cease if all the substrate is used up. An (a, h) system obtains similar properties if the autocatalysis saturates moderately.

C. Biochemical switches

A monotonic gradient based on the mechanisms described above can be maintained only if the size of the tissue is small, since otherwise the time required to exchange molecules by diffusion from one side of the field to the other would become too long. Indeed, as Wolpert (1969) has pointed out, all biological systems in which pattern formation takes place are small, less than 1 mm and less than 100 cells in diameter. In an organism growing beyond this size, cells have to make use of the signals they have obtained by activating particular genes. Once triggered, the gene activation should be independent of

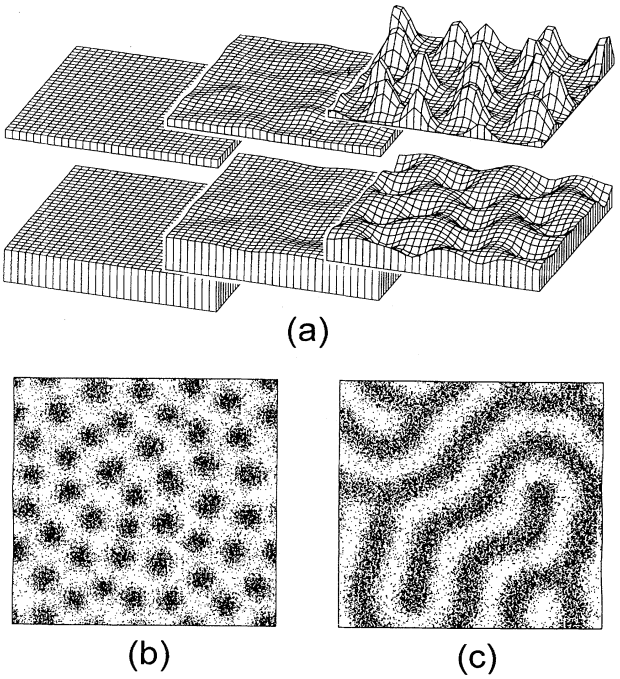

FIG. 2. Patterns produced by the activator-substrate model (3). (a) Initial, intermediate, and final pattern. Upper and lower plots show the concentrations of a and s, respectively. A high level of a produces a pit in the distribution of the substrate s. (b) Similar simulation in a larger field (the activator concentration is shown). Figures 1 and 2 have been calculated with corresponding parameters. Nevertheless the peaks here are broader and more densely packed. (c) Saturation of the autocatalysis ($\kappa_a > 0$) leads to the formation of stripes.

the evoking signal. Similarly to pattern formation, this requires either a direct or an indirect autocatalytic activation of genes (Meinhardt, 1978).

Here is a simple example of a switch system:

$$\frac{\partial y}{\partial t} = \rho_y \frac{y^2}{1+\kappa_y y^2} - \mu_y y + \sigma^{\text{ext}} . \tag{5}$$

In this equation ρ_y, μ_y, and κ_y are constants; σ^{ext} describes the external signal. In the absence of such a signal the system has two stable steady states, the low one at $y = 0$ and the high one at $y = (\rho_y + \sqrt{\alpha})/2\kappa_y\mu_y$, separated by an unstable steady state at $y = (\rho_y - \sqrt{\alpha})/2\kappa_y\mu_y$, where $\alpha = \rho_y^2 - 4\kappa_y\mu_y^2$. If the external signal σ^{ext} exceeds a certain threshold the system switches from the low to the high state (Fig. 3). Once the unstable steady state is surpassed, the high state will be reached and maintained independently of the external signal (which could even vanish).

Somewhat more complex interactions allow the space-dependent activation of several genes under the influence of a single gradient (Meinhardt, 1978). Meanwhile many genes have been found with a direct regulatory influence on their own activity (see, for instance, Kuziora and McGinnis, 1990; a review is given by Serfling, 1989), supporting the view that autoregulation is an essential element in the generation of stable cell states in development.

D. Other realizations of local autocatalysis and long-range inhibition

In the above-mentioned models, self-enhancement occurs by direct autocatalysis (the activator production term in $\partial a/\partial t$ is proportional to a^2). This direct feedback is not necessary. As already mentioned, self-enhancement may also result from indirect mechanisms. As an example, consider the following system:

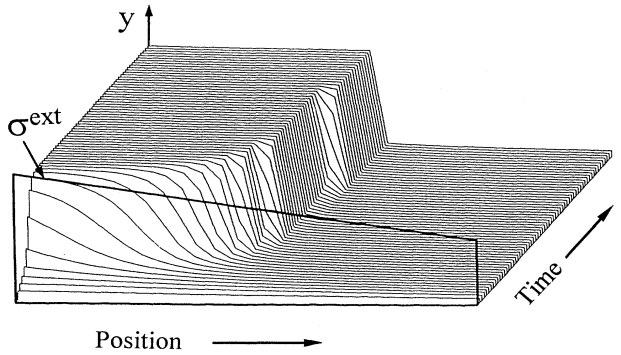

FIG. 3. Position-dependent activation of a gene by an external signal simulated in a one-dimensional array of cells according to Eq. (5). The concentration of the autoregulatory gene product y (fine lines) is given as a function of position and time. A primary gradient (boldface line) is used as external signal σ^{ext}. Despite the shallow signal, a sharp threshold exists; if it is exceeded, the system switches irreversibly to the high state.

$$\frac{\partial a}{\partial t} = D_a \triangle a + \rho_a \left(\frac{c}{1+\kappa_a b^2} - a \right) + \sigma_a , \tag{6a}$$

$$\frac{\partial b}{\partial t} = D_b \triangle b + \rho_b \left(\frac{1}{1+\kappa_b a^2 c} - b \right) + \sigma_b , \tag{6b}$$

$$\frac{\partial c}{\partial t} = D_c \triangle c + \rho_c \, (b - ac) . \tag{6c}$$

In this example the two substances a and b mutually repress each other's production. A small local advantage of a leads to a decrease in production of the b. If b shrinks, a increases further, and so on. In this case, self-enhancement results from the local repression of a repression. The necessary long-range inhibition is mediated by the rapidly diffusing substance c, which is produced by b but is poisonous to it. Further, c is removed with the help of a. So, although a and b are locally competing, a needs b in its vicinity and vice versa. Therefore the preferred pattern generated by such a system consists of stripes of a and b, closely aligned with each other.

The interaction given above is a simple example of an important class of pattern-forming reactions based on long-range activation of cell states that locally exclude each other (Meinhardt and Gierer, 1980). According to the theory, they play an essential role in the segmentation of insects (Meinhardt, 1986). Molecular analysis has confirmed this scheme; the *engrailed* and the *wingless* genes of *Drosophila* have the predicted properties [see, for instance, Ingham and Nakano (1990) or Ingham (1991)].

The examples discussed here have been selected from a large set of feasible morphogenetic models (Gierer, 1981). They have the advantage of conceptual simplicity. Many other nonlinear systems have been proposed (Lacalli, 1990; Lyons and Harrison, 1992; for a broad overview, see Murray, 1990). But, to state it once again, more important than the details of the equations are the basic principles on which all these models rely, on *local self-enhancement* and *long-range inhibition.*

Numerical simulations have shown that properties of the systems discussed above are able to account for many observations. As an example, regeneration after tissue removal will be discussed further below.

The models presented describe biochemical reactions and diffusion of the reactants. Other kinds of interactions are possible, mediated for instance by mechanical forces (Lewis and Murray, 1992; Bentil and Murray, 1993), by electric potentials (Jaffe, 1981; Stern, 1986), or by surface contact between cell membranes (Babloyantz, 1977). Cellular automata are also often used to explain the emergence of inhomogeneous patterns (Cocho *et al.*, 1987); they provide particularly elegant solutions as long as only cell-cell contacts are involved (i.e., the state of a cell affects only its direct neighbors). However, chemical interactions coupled by the exchange of molecules (either by diffusion or by more complex signaling mechanisms) are believed to be the main motor of primary pattern genesis in biological systems.

IV. SOME REGULATORY PROPERTIES OF PATTERN-FORMING REACTIONS

In the previous section, we discussed some simple models able to produce inhomogeneous concentrations of chemicals out of a (nearly) homogeneous initial state. Let us now observe the main characteristics of the resulting patterns.

A. Insertion of new maxima during isotropic growth

Suppose that the initial field is large when compared with the range of the inhibitor. If the pattern is initiated by small random fluctuations, the inhomogeneous steady state of an activator-inhibitor model consists of irregularly arranged activator peaks. Due to lateral inhibition, each peak maintains a certain minimal distance from its neighbors.[3]

If the field grows isotropically (Fig. 4), new activator maxima emerge at positions where the inhibitor is too low to further repress the local onset of autocatalysis from the basic activator production. This requires a minimum distance from existing activated centers. Therefore the average spacing and the overall density of maxima remain approximately constant.

Biological examples of such near-periodic patterns are the distribution of stomata (special organs for gas exchange) on the lower surface of leaves (Bünning and Sagromsky, 1948) or the arrangement of bristles on insect cuticle (Wigglesworth, 1940). In both cases, it has been demonstrated that during growth new structures arise where the old ones are the most widely spaced [Fig. 4(b)].

B. Strictly periodic patterns

To get strictly periodic patterns, one needs more subtle mechanisms. The simplest idea would be to achieve strict periodicity by relaxation of a random structure. However, this is unrealistic from a biological point of view. Relaxation takes time. A misplaced maximum may already evoke a particular structure, for instance a bristle, at the wrong position. This cannot be corrected by a later shift of the maximum to the correct place.

Strictly regular structures are formed during marginal growth. With the addition of new cells at the boundaries, the distance between these cells and the existing maxima increases and the inhibitor concentration decreases. Whenever the inhibitor concentration becomes lower than some threshold a new maximum is triggered. Therefore each new maximum keeps a well defined distance from the previously formed ones, and the arrangement is very regular (Fig. 5).

A famous example of the generation of a strictly periodic structure is the initiation of leaves on a growing shoot. As the shoot grows upward, new leaves (or florets, scales, etc.) are added sequentially near the tip, so as to maximize the spacing with the older ones (Adler, 1975; Marzec and Kappraff, 1983). Leaves emerge along spirals [Fig. 5(b)] that wrap around the stem (Coxeter, 1961; Rothen and Koch, 1989a, 1989b). We shall come back to this particular pattern in Sec. V.

It may also happen that systems which have already reached a large size need to position organs in a regular fashion. This can occur by a "simulated" growth. The property of a tissue may change in a wavelike manner from a noncompetent to a competent state for pattern formation. Although many cells are already present, pattern formation can take place only in a small portion of the field. With the enlargement of the competent region more and more maxima are formed that keep a precise distance from the existing ones. An example is the formation of the regularly spaced feather pattern in chicks [Fig. 5(c)]. Feather primordia begin their differentiation behind a competence wave that starts from the dorsal midline and spreads to both sides of the back. Experiments (Davidson, 1983a, 1983b) have clearly demonstrated that lateral inhibition is involved in the formation of the regularly spaced feather primordia. We shall meet a similar phenomenon in Sec. V when discussing the formation of the *Drosophila* eye.

C. Regeneration properties and polarity

Many biological systems can regenerate missing parts. The models discussed above are able to account for this property. We shall use the activator-inhibitor model and modifications of it to demonstrate this feature and compare them with biological observations.

After partition of an early sea urchin embryo both fragments regenerate complete embryos. By vital staining during separation it has been shown that both embryos obtain a mirror-image orientation with respect to each other (Fig. 6). According to the model, in a nonactivated fragment the remnant inhibitor decays until a new activation is triggered. The polarity of the resulting pattern depends on the distribution of the residual activator and inhibitor in the fragment. A polarity reversal, as in the case of the sea urchin mentioned above, will take place if the residual inhibitor gradient is decisive for its orientation. It is the region with the lowest inhibitor concentration, i.e., the region most distant from the originally activated site that wins the competition to become activated.

In many other systems the polarity is maintained. The fresh water polyp *Hydra* (Wilby and Webster, 1970; Wolpert *et al.*, 1971; Macauley-Bode and Bode, 1984) and planarians (Flickinger and Coward, 1962; Goss, 1974; Chandebois, 1976) are examples. The maintenance of po-

[3]The mean distance d between two neighboring maxima can be evaluated by use of the wave number $k_{\max}$ calculated in the linear approximation [see Appendix A, Eq. (A6)]: $d \approx 1/k_{\max}$.

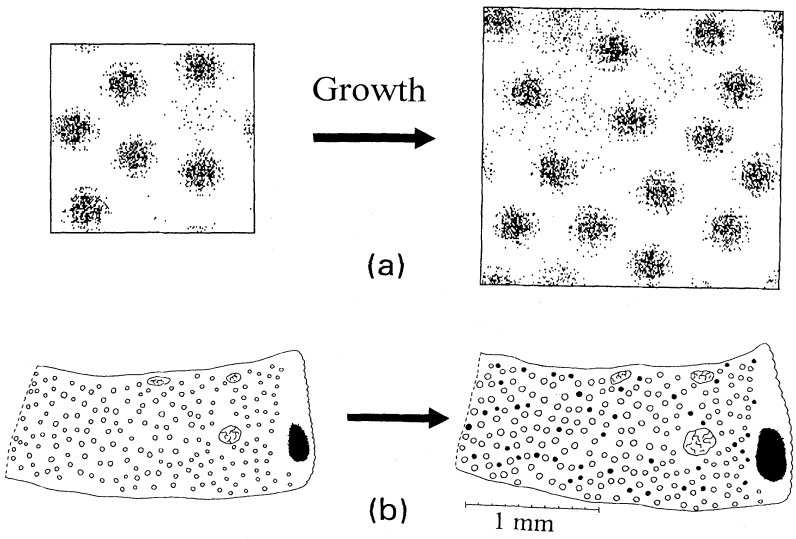

FIG. 4. Insertion of new maxima during growth: (a) During isotropic growth, the distance between the maxima enlarges and the inhibitor concentration drops in between. Whenever the inhibition becomes too weak, a new maximum is triggered. This can only occur if a minimum distance from existing maxima is respected. The figure is calculated with an (a, h) model and shows the activator concentration. (b) Example for the insertion of new structures during growth: the distribution of bristles on the cuticle of a bug *Rhodnius prolixus* (after Wigglesworth, 1940). The drawings correspond to the fourth (left) and fifth (right) larval instars, respectively. Bristle positions are marked with circles (○); during growth, new bristles (•) appear where the old ones are the most widely spaced.

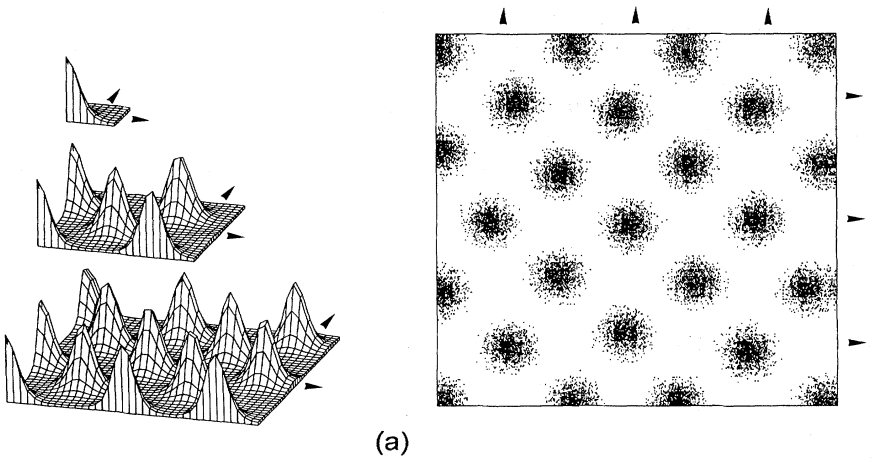

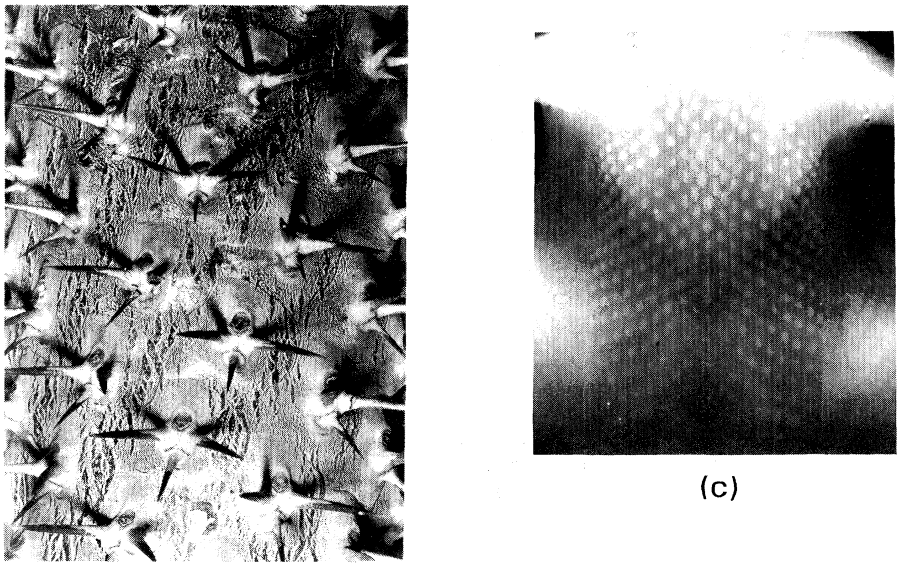

FIG. 5. Generation of periodic structures during marginal growth: (a) In this simulation, the domain enlarges by addition of new cells at the upper and left borders; a periodic structure emerges. Plotted is the activator of an (a, h) model. (b) The regular spacing of thorns on this cactus is achieved by apical growth (see also Sec. V). The thorns are arranged along helices that wrap around the stem. (c) Feather primordia are regularly spaced on the back of a chicken. To position them accurately, the chicken "simulates" growth by use of a determination wave that starts from the dorsal midline and spreads on both sides: only cells reached by the wave can initiate the development of primordia. The wave motion simulates growth by enlarging the region competent for feather production (photograph by courtesy of Dr. H. Ichijo).

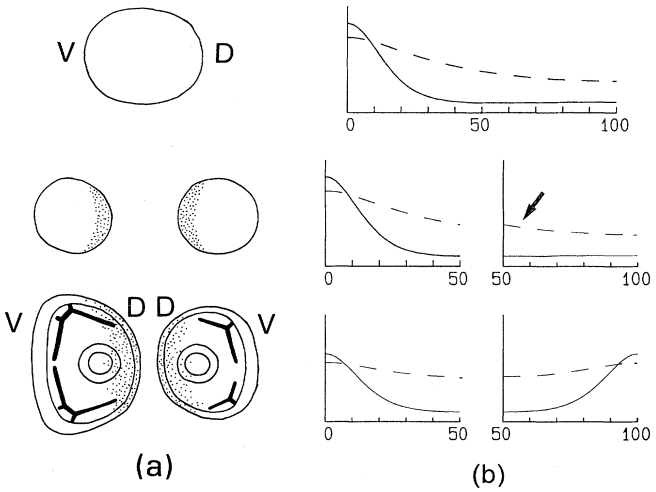

FIG. 6. Regeneration with polarity reversal: (a) Experimental observation. The early blastula of a sea urchin is cut in two halves. Cells close to the wound are vitally stained (dotted region) to determine later the original orientation. Both parts regenerate a complete embryo. They are mirror symmetric, so that in one fragment the polarity must have been reverted (Hörstadius and Wolsky, 1936). (b) Simulation by an activator-inhibitor model. The abscissa scale gives the position along the dorso-ventral axis of the blastula, in percent of the animal length. After separation, the high residual inhibitor concentration (dashed curve) in the nonactivated part (arrow) leads to regeneration of the activator (solid curve) at the opposite end of the field. The distribution before and after cutting is shown, as well as the newly formed steady state.

larity implies that the same tissue can regenerate either a head or a foot depending whether this particular tissue is located at the apical or the basal end of the fragment which has to regenerate. Morgan (1904) interpreted this phenomenon as evidence that a graded stable tissue property exists. It provides a graded advantage in the race to regenerate a removed structure. During head regeneration, for instance, those cells will win that were originally closest to the removed head.

In terms of the activator-inhibitor mechanism, a systematic difference in the ability to perform the autocatalysis must exist. We call this property the *source density*. Detailed simulations for hydra (Meinhardt, 1993) have shown that the source density must have approximately the same slope as the inhibitor. However, while time constants of the activator and inhibitor are in the range of a few hours, a major change of the source density requires approximately two days (Wilby and Webster, 1970).

In the following model, a feedback exists from the inhibitor h onto the source density b. Therefore, in the course of time, a long-range gradient not only of h but also of b will be established. Whenever the system is forced to regenerate, the residual distribution of b ensures the maintenance of polarity.

$$\frac{\partial a}{\partial t} = D_a \triangle a + \rho_a \left[b \left(\frac{a^2}{h^2} + \sigma_a \right) - a \right] , \qquad (7a)$$

$$\frac{\partial h}{\partial t} = D_h \triangle h + \rho_h \left(a^2 - h \right) , \qquad (7b)$$

$$\frac{\partial b}{\partial t} = \rho_b \left(h - b \right) . \qquad (7c)$$

As can be verified in Eq. (7c), at equilibrium, $b = h$. Thus the self-enhancement term ba^2/h^2 in the activator equation (7a) reduces to a^2/h, as in the usual activator-inhibitor model [Eq. (1)]. Since the removal rate ρ_b is small compared to ρ_a and ρ_h, b preserves the polarity when the animal is dissected: due to enhancement of autocatalysis by b, the activator a builds up again in each half at the site of highest b concentration. The position of the *relative* highest source density plays the crucial role in determining where the new activator maximum will be formed. This insures maintenance of the initial polarity (Fig. 7).

The feedback of h onto the source density b has another very important effect; it helps to suppress the initiation of secondary maxima. This is required if a single structure, for instance a single head, should be maintained in a system despite substantial growth. Since, with increasing distance from the existing maxima, cells have a lower and lower source density, it becomes less likely that these cells will overcome the inhibition spreading from an existing maximum.

In *Hydra*, treatment with diacylglycerol (a substance

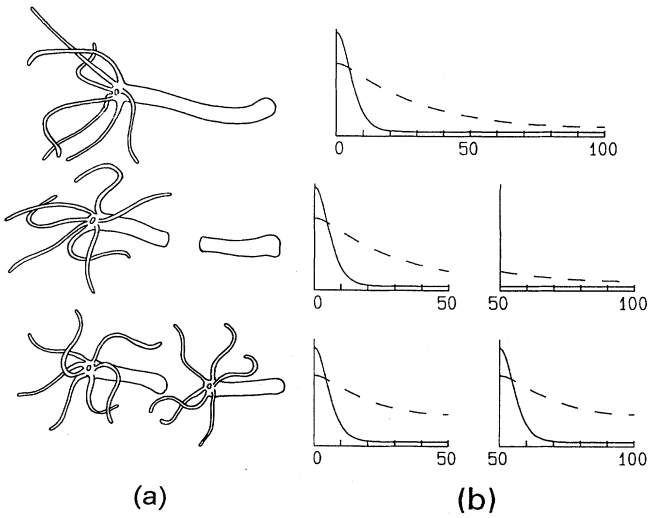

FIG. 7. Regeneration with maintained polarity. (a) After cutting, fragments of *Hydra* regenerate. The original apical-basal polarity is maintained. (b) Model based on Eq. (7). The abscissa gives, in percent of the full length, the position along the body axis. The inhibitor is assumed to have a feedback on the source density b (dashed curve) which describes the general ability of the cells to perform the autocatalysis. This source density, having a long time constant, does not change very much during regeneration of the activator-inhibitor pattern. Regions closer to the original head have an advantage in the competition for head formation, and the new maximum of the activator a (solid curve) is reliably triggered in the region that was originally closest to the apical side.

involved in the second messenger pathway) causes supernumerary heads (Müller, 1990). From detailed observations and simulations one can conclude that this substance is able to increase the source density in a dramatic way. Since the source density becomes high everywhere, the so-called apical dominance of an existing head is lost and supernumerary heads can be formed. These heads keep their distance from each other since the spacing mechanism enforced by the inhibitor alone is still working. The model agrees with many other experimental results, including the existence of a critical size (see Appendix A) below which the animal is unable to regenerate (Shimizu *et al.*, 1993).

V. FROM SIMPLE GRADIENTS TO COMPLEX STRUCTURES

So far we have considered models able to generate inhomogeneous distributions of substances out of an initially uniform state. When several systems of this kind are combined, very complex structures can be formed in a reproducible way. Central to this process is the idea of *hierarchy*. A first system A establishes a primary pattern that is used to modify and trigger a second system B. The feedback in the reverse direction, of B onto A, is assumed to be weak (this greatly simplifies the treatment of these nonlinear systems and makes the comprehension of their properties easier).

Suppose that both A and B are activator-inhibitor systems (a_A, h_A) and (a_B, h_B). It is then natural to assume that parameters ρ_{a_B}, ρ_{h_B}, σ_{a_B} ,... of B are functions of the chemical concentrations of A. The couplings which have proved to be the simplest and the most efficient in simulations modify either the cross-reaction parameter ρ_{a_B} or the basic (activator-independent) production σ_{a_B} of the second activator a_B. The two following rules of thumb are helpful:

(i) If the second system has to respond dynamically to any change in the first one, one will preferentially alter the value of ρ_{a_B}. This ensures that any change in A is carried over to B [in terms of Fig. 14 in Appendix A, one would choose the coupling function ρ_{a_B} in such a way that the system B shifts under the pressure of A from the region H of the stability diagram (where B has no pattern formation ability) into the domain I (where inhomogeneities can be amplified)].

(ii) If A has only to trigger B, the coupling between the two systems is achieved by the basic production σ_{a_B}. The structure developed by B is then stable even if, later, A vanishes.

Other kinds of interactions are conceivable as well. For instance, cells could change the communication with their neighbors by opening or closing gap junctions; this can be modeled by altering the diffusion constants under the influence of a second patterning system. In the four examples developed below, however, we restrict the interaction between systems to the two rules mentioned above. The first two systems are relatively simple models for animal coat patterns and for reticulated structures. The last two examples are more complex and describe interactions that lead to the precise arrangement of differently determined cells in a strictly periodic way. The eye formation in *Drosophila* and organ genesis in a growing plant will be used as biological counterparts.

A. Animal coat patterns

The variability and complexity of animal coat patterns has attracted many biologists. Models can be found for the coloration of butterfly wings (Nijhout, 1978, 1980; Murray, 1981a), zebra stripes (Bard, 1981; Murray, 1981a, 1981b), patterns on snake skin (Cocho *et al.*, 1987; Murray and Myerscough, 1991), or on sea shells (Meinhardt and Klinger, 1987; Ermentrout *et al.*, 1986). We present here a simple reaction-diffusion mechanism which allows widely varying patterns, ranging from the spots of the cheetah to the reticulated coat of the giraffe.

In mammals, hair pigmentation is due to *melanocytes*, which are supposed to be uniformly distributed in the derma. Whether they produce melanin (which colors hairs) or not is believed to depend on the presence of some unknown chemicals whose pattern is laid down during the early embryogenesis (Bard, 1977).

Let us start with a short description of the giraffe's coat. Figure 8 shows the similarity between the polygonal spots that cover the animal and Dirichlet domains. This suggests that a reaction-diffusion system is at work in the giraffe's coat that is able to produce Dirichlet polygons. Consider a surface $\mathcal{S}$ and points $P_1, \ldots, P_n$ randomly scattered on it. Suppose that each P_i initiates at a given time a chemical wave, which spreads uniformly in all directions. The system should be such that, if two waves meet, they annihilate each other. The lines along which annihilation occurs define the envelopes of the Dirichlet domains around the initial centers P_i. The following reaction-diffusion system fulfills these requirements:

$$\frac{\partial a}{\partial t} = D_a \triangle a + \rho_a \left[\frac{a^2 s}{1+\kappa_a a^2} - a \right] , \tag{8a}$$

$$\frac{\partial s}{\partial t} = D_s \triangle s + \frac{\sigma_s}{1+\kappa_s y} - \frac{\rho_s a^2 s}{1+\kappa_a a^2} - \mu_s s , \tag{8b}$$

$$\frac{\partial y}{\partial t} = \rho_y \frac{y^2}{1+\kappa_y y^2} - \mu_y y + \sigma_y a . \tag{8c}$$

One recognizes a modified activator-substrate model (a, s) combined with a switching system y. Melanocyte activity is given by y, where $y = 1$ corresponds to cells producing melanin, while $y = 0$ corresponds to calls that do not. The state y of each pigment cell is determined by its exposure to the morphogen a. To insure that a does not produce a stationary pattern but spreads like a wave, the diffusion constant of s should not be too large when compared to that of a.

The system works in the following way: initially $y = 0$, $a = 0$, and $s = s_0$ everywhere, except at some randomly

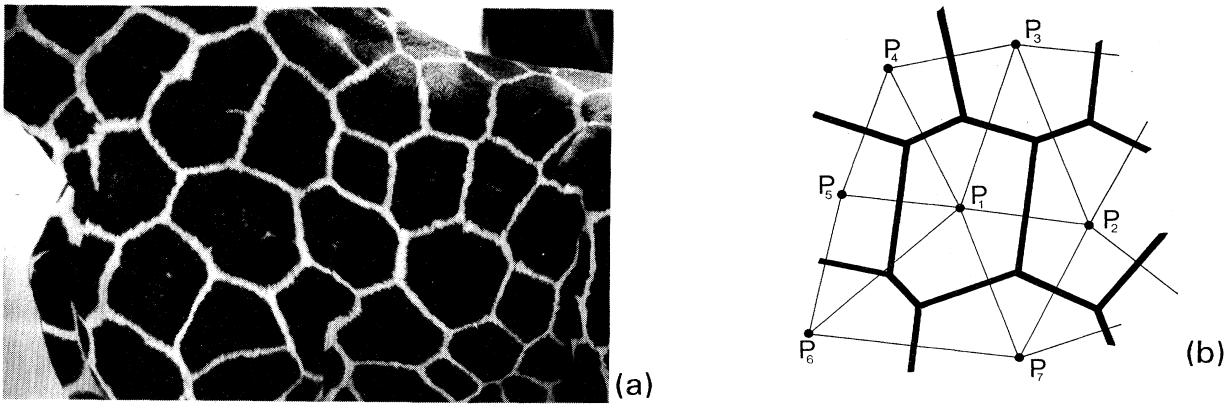

FIG. 8. Analogy of the giraffe pattern with Dirichlet domains. (a) Side of a giraffe (*Giraffa camelopardalis reticulata*). The pattern is formed by convex polygons separated by thin lines (photograph kindly provided by O. Berger). The formal resemblance with Dirichlet domains is suggestive. (b) Construction and definition of Dirichlet domains. Given a set $\{P_1, \ldots, P_n\}$ of points belonging to a surface $\mathcal{S}$, one draws the perpendicular bisectors between neighboring points. The convex envelop surrounding a center P_i delimits its associated Dirichlet domain $\mathcal{D}_i$. By construction, $\mathcal{D}_i$ contains all the points of the surface $\mathcal{S}$ nearer to P_i than to any other P_j $(j \neq i)$.

scattered points[4] P_i, where $a = a_0$; this high value of a switches y from 0 to 1 at P_i due to the source term $\sigma_y a$ in Eq. (8c). On the other hand, due to the depletion of s and to its low diffusion constant D_s, high-a regions shift toward zones where the substrate is abundant: a waves propagate over the surface. When two such waves get close, they annihilate each other due to the depletion of substrate s. Owing to its switching nature, y needs the activator a in order to be triggered. Once a has vanished, the state of y remains stable. Note that y has a negative feedback on the production of s in Eq. (8b); in regions where y has switched on, it is no longer necessary to waste energy to produce the substrate s any more.

Figure 9(a) presents the result of a simulation. The similarity to the coat of a giraffe is obvious. Straight lines with nearly constant thickness delineate irregular polygons; earlier models proposed for giraffe patterns (Murray, 1981a, 1981b, 1988) produce, instead, spots comparable to Fig. 9(c).

According to the parameter values, model (8) produces a variety of patterns related to Dirichlet domains. For instance, if the removal rate of s is low enough, regions where a does not vanish remain; the system then reaches a stable configuration in which the activator a remains activated along circular rings or "half-moons" centered on the initiating points P_i [Fig. 9(b)]. Conversely, if the consumption of s is too high, the a waves cannot spread very far and die before they meet; forming randomly scattered spots [Fig. 9(c)]. In that situation, the resulting pattern has many similarities to the one described by Murray (1981a, 1981b, 1988).

[4]In principle the centers P_i could be laid down by a primary pattern-formation mechanism (a_P, h_P) like that used to produce Fig. 1(a). These points would then activate the production of a by means of an additional term $\sigma_a a_P$ in Eq. (8a). We skip this step.

The coats of mammals have been taken as illustrations. Fish, snakes, and insects show similar patterns. It is appealing to imagine that they may all be based on a common mechanism involving Dirichlet domains, as discussed above.

B. Reticulated structures

Polygonal patterns are also common in other biological systems. The fine veins of the wing of a dragonfly or the projection areas of mice sensory whiskers on the brain are examples (Fig. 10).

A crucial property of the system discussed in the preceding paragraph is that the pattern, once formed, is fixed. For instance, no new lines can be inserted during growth to subdivide a large polygon into two smaller ones. This is appropriate for the giraffe's coat as indicated by the large size of the polygons. For other systems, such as the wing of the dragonfly mentioned above, it is to be expected that the final pattern is not produced in a single step at a particular moment of the development. Rather, it is likely that, at an early stage and in a small field, a simple pattern is laid down. We assume that, in analogy to the *Drosophila* wing venation (Diaz-Benjumea *et al.*, 1989; Garcia-Bellido *et al.*, 1992), the positions of the main veins of the dragonfly wing are genetically determined; the finer ones are presumably added later in order to strengthen the growing structure and to keep approximately constant the size of a domain enclosed by veins.

The following model has this property. It relies upon hierarchical interactions of two systems. A first (a, s) activator-substrate system produces a pattern of activator mounds [see Fig. 2(a)]:

$$\frac{\partial a}{\partial t} = D_a \triangle a + \rho_a \left(\frac{s a^2}{1 + \kappa_a b^2} - a \right) + \sigma_a \ , \tag{9a}$$

$$\frac{\partial s}{\partial t} = D_s \triangle s - \rho_s \left(\frac{s a^2}{1 + \kappa_a b^2} \right) + \sigma_s \ . \tag{9b}$$

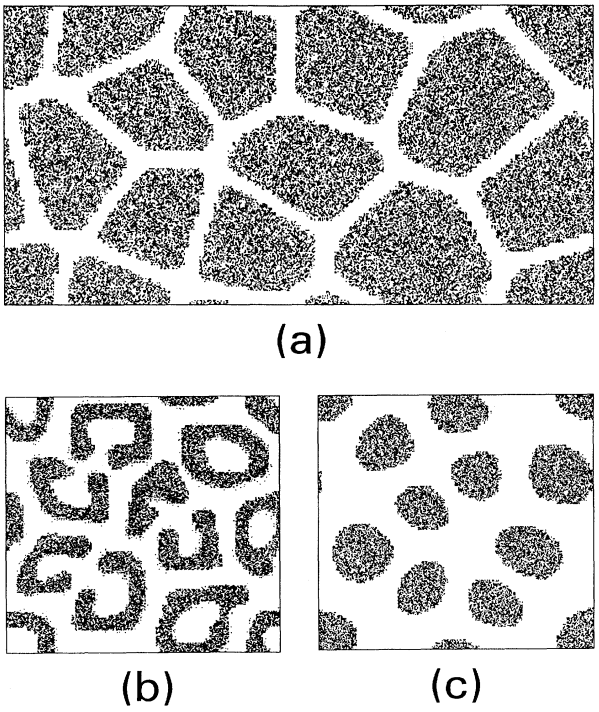

FIG. 9. Simulation with the system (8). The dot density is proportional to the concentration of y. According to the parameter set, the resulting pattern will have similarities with that observed on the coats of (a) giraffes (*Giraffa camelopardalis reticulata*), (b) leopards (*Panthera pardus*), or (c) cheetahs (*Acinonyx jubatus*).

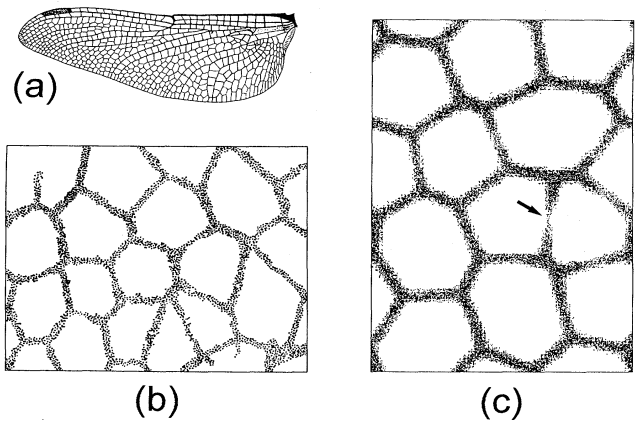

FIG. 10. Polygonal structures: (a) The left posterior wing of a dragonfly (*Libellula depressa*) is strengthened by a fine and elegant network of veins (picture after Séguy, 1973). The positions of the larger veins are presumably genetically coded. According to the model, finer veins are produced during wing development: During growth, their insertion tends to keep constant the size of the enclosed domains. (b) Experimentally observed barrel pattern in the mouse somatosensory cortex. The dotted regions correspond to domains labeled by an antibody against J1/tenascin (after Steindler *et al.*, 1989). (c) Simulation based on the system (9)–(10) in a two-dimensional domain. The density of dots is proportional to the concentration of b. One can see the completion of a new boundary between two domains (arrow).

This primary pattern triggers an activator-inhibitor system (b,h) producing boundaries around the mounds of a:

$$\frac{\partial b}{\partial t} = D_b \triangle b + \rho_b \left[\frac{s^2}{1+\kappa_b a b^2} \left(\frac{b^2}{h} + \sigma_b \right) - b \right] , \quad (10a)$$

$$\frac{\partial h}{\partial t} = D_h \triangle h + \rho_h \left(b^2 - h \right) . \quad (10b)$$

The a concentration modifies the saturation value of the activator b in Eq. (10a). A high value of a makes this saturation so strong that the (b,h) system is set off. In regions of low a, the process is reversed: the saturation becomes weak enough so that the (b,h) system triggers the formation of a stripelike boundary. This effect is enhanced by the substrate s, through the term $\rho_b s^2$ in Eq. (10a). In other words, stripes will appear along sites with a high concentration of s, in regions that are most distant from the maxima of a. Due to the action of h, the stripes become sharp. The weak feedback of b onto a in Eq. (9a) is not absolutely necessary but speeds up the development of the structure.

The model has size regulation properties. New boundaries are inserted whenever a domain becomes too large. This is because, with growth, the distance between the a maxima increases. If a certain distance is surpassed, a maximum splits into two and displacement towards a higher substrate concentration follows. Between these two maxima, a new region with high substrate concentration appears that, in turn, initiates a new b line. Such a process can be observed in Fig. 10(c).

As a possible application of the mechanism (9)–(10) let us briefly mention the barrel formation in the brain of a mouse (Steindler *et al.*, 1989; Jacobson, 1991). The facial vibrissae of the mouse project on the primary somatosensory cortex [Fig. 10(b)]. The mapping on the brain mirrors the arrangement of whiskers on the mouse's face: two adjacent vibrissae project on neighboring sites in the cortex; the domain connected to a given whisker is called a *barrel*. The shape of the barrels can be highlighted by a labeling with tenascin-specific antibodies.[5] During the first postnatal days, the barrel pattern has dynamic properties: removal of vibrissae disrupts the formation of the associated barrels. The model gives a good description of such dynamic effects if one admits that the autocatalytic production rate of activator a is linked to neural excitation by the whiskers. Destruction of the latter leads to a reduction of neural excitation, to a decrease of a, and so to the resorption of the associated barrel, whose area is then invaded by its neighbors.

[5]An important component of biological tissue is the extracellular matrix, an entanglement of macromolecules that strengthens the cellular structure. Tenascin is a glycoprotein involved in the adhesion of neurons to the extracellular matrix. The local concentration of tenascin can be visualized by staining it with specific fluorescent-labeled antibodies.

C. The faceted eye of *Drosophila* flies

As an example of a complex but very regular periodic structure, we shall now discuss the formation of the faceted eye of the fruit fly *Drosophila melanogaster*. The eye is derived from the *eye-antennal imaginal disk*.[6] It consists of a very regular array of about 700 ommatidia [Fig. 11(a)]. Each ommatidium is formed by the precise arrangement of 20 cells, among which 8 are photoreceptor neurons named *R1, ..., R8*. These clusters of 20 cells have well defined polarity and orientation with respect to the main body axis.

The molecular basis of eye formation has been extensively studied over the last few years. For comprehensive reviews, see, for instance, Tomlinson (1988) or Basler and Hafen (1991). The model presented below reproduces essential aspects of this pattern formation.

The following steps play a crucial role [Fig. 11(b)].

(a) A wave moves from posterior to anterior across the eye imaginal disk. It causes a slight deformation in the tissue, the *morphogenetic furrow*.

(b) Within the furrow, a first morphogenetic event takes place. It leads to the formation of regularly spaced clusters of six or seven cells, including one *photoreceptor neuron* $R8$ and one or two *mystery cells* M.

(c) In the cluster around $R8$, three pairs of photoreceptors differentiate sequentially, first $R2$ and $R5$, then $R3$ and $R4$, followed by $R1$ and $R6$; finally, $R7$ is formed. During this stage, the mystery cells M are eliminated by selective cell death.

(d) Finally the cluster of eight photoreceptors recruits other cells in order to form the cone, pigment, and bristle cells.

The eight photoreceptors $R1$–$R8$ belong to at least three types, namely, $R1$–$R6$, $R7$, and $R8$. Receptors $R7$ and $R8$ have clearly distinct functions, as appears from their morphology (Tomlinson, 1988). Whether $R1$–$R6$ are different is unclear (Heberlein *et al.*, 1991). The differentiation pathways show that there are three pairs of similar receptors, $R1/6$, $R2/5$, and $R3/4$. If the six neurons $R1$–$R6$ are functionally identical, a plausible reason for their sequential differentiation is to achieve a precise regulation of the number of photoreceptors contained in each ommatidium (differentiating them in one step could lead to an irreproducible receptor number).

The fate of a cell is determined only by interactions with its neighbors, and not by its lineage (Ready *et al.*, 1976). The system is therefore very convenient for studying the interactions required to achieve a complex periodic structure. Moreover, the pattern formation takes place in a monolayered epithelium; it is a strictly two-dimensional process.

We propose here a model that accounts for the first morphogenetic steps up to the formation of the $R1$ and $R6$ receptors. The fate of the cell is assumed to be hierarchically determined in a cascade:

$$\text{furrow} \longrightarrow R8 \text{ cells} \longrightarrow M \text{ cells} \longrightarrow R2/5 \text{ cells} \longrightarrow \cdots .$$

In the following, a model for each individual step will be described. The hierarchical interactions postulated are summarized in Fig. 12(a).

1. The morphogenetic furrow

The differentiation of cells behind a spreading wave indicates that, in the eye, the precise arrangement of structures is achieved by the scheme of simulated growth mentioned in Sec. IV. In this way, each subsequently formed structure achieves a precise spacing with respect to the structures already laid down.

The morphogenetic furrow is modeled as a wavelike event which moves across the system. This is in agreement with the experiments of White (1961), where grafting of epithelium tissue in the eye imaginal disk of mosquitoes allowed him to observe the furrow spreading through holes of the grafted tissue or moving around it like a wave.

The following equations have been used to simulate the wave that generates the furrow:

$$\frac{\partial f}{\partial t} = D_f \triangle f + \rho_f \frac{s f^2}{1 + \kappa_f f^2} - \mu_f f \ , \tag{11a}$$

$$\frac{\partial s}{\partial t} = -\rho_s s f^2 \ . \tag{11b}$$

Suppose that initially $s = 1$ and $f = 0$ everywhere, except in one cell where $f = f_0$. Due to diffusion, this cell activates the production of f in its vicinity [the term $D_f \triangle f$ in Eq. (11a) plays the role of σ^{ext} in (5)]. But, since the substrate s is depleted, f cannot remain in its high state and goes back to zero. This produces a wave front of f, which spreads once over the eye disk.

The furrow model (11) is certainly a simplification. It does not match all experimental data. A shift of fly embryos to nonpermissive temperatures halts the motion of the furrow. When shifted back to normal temperatures, the furrow continues as if nothing had happened. The model is not well suited to reproduce this experiment: it would require a simultaneous decrease of ρ_s and of D_f. The change of both parameters at the same time by the temperature shift is unlikely and indicates a more complex wave formation. For our purpose, however, the form (11) is sufficient, since we only need it as a signal for beginning the neuronal differentiation.

2. The $R8$ photoreceptors

The morphogenetic wave triggers the differentiation of neuronal cells $R8$. Experimental data indicate that lateral inhibition is essential for proper $R8$ spacing (Baker *et al.*, 1990; Harris, 1991), so $R8$ cells are best modeled by an activator-inhibitor couple (a_{R8}, h_{R8}):

$$\frac{\partial a_{R8}}{\partial t} = D_{a_{R8}} \triangle a_{R8} + \rho_{a_{R8}} \left(\frac{a_{R8}^2}{h_{R8}} - a_{R8} \right) + \sigma_{a_{R8}} f \ , \tag{12a}$$

[6] In *Drosophila* larvae, *imaginal disks* are nests of epithelial tissue which differentiate at metamorphosis. Legs, wings, antennae, eyes derive from imaginal disks (Alberts *et al.*, 1989).

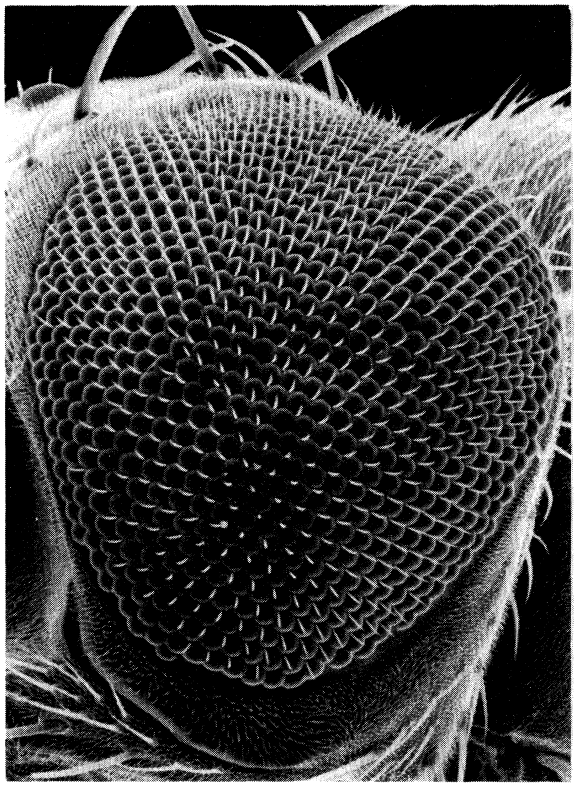

(a)

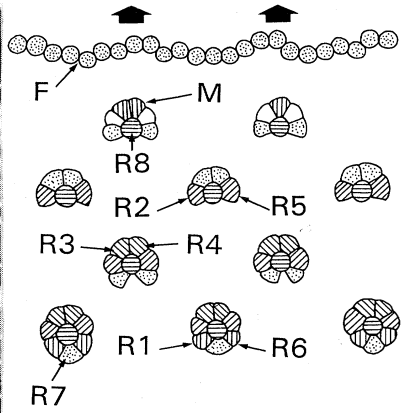

(b)

FIG. 11. Overall structure of the *Drosophila* eye and its genesis: (a) Scanning electron micrograph of the eye of a *Drosophila* fly showing the regular array of ommatidia (photograph kindly provided by J. Berger). (b) Pattern formation of the *Drosophila* eye. A morphogenetic furrow F sweeps anteriorly across the eye-antennal imaginal disk (the arrows show the direction of propagation). Behind the furrow, ommatidial assembly begins with the differentiation of regularly spaced $R8$ photoreceptors, each one associated with one or two mystery cells M. Later $R2$ and $R5$ neurons are recruited, followed by the formation of $R3$, $R4$, $R1$, $R6$, and, finally, $R7$ receptors; M cells are meanwhile eliminated by selective cell death. After formation of all photoreceptors, 12 other cells are added in every ommatidium (cone, pigment, and bristle cells). Dots indicate differentiating cells while hatches show differently differentiated cells.

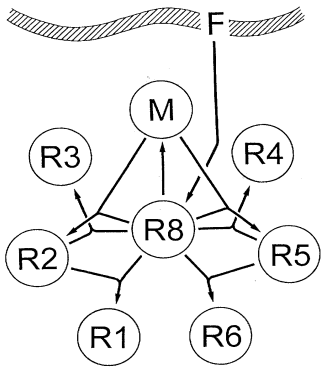

(a)

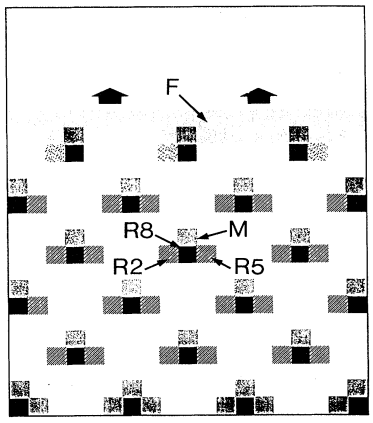

(b)

FIG. 12. Simulation of eye development. (a) Scheme of hierarchical interactions used in the model. The furrow F induces regularly spaced $R8$ neurons. These are needed to develop M cells. Later, $R8$ and M cells cooperate to trigger the differentiation of $R2$ and $R5$ neurons. Finally, $R8$ and $R2/5$ neurons induce the formation of $R3/4$ and $R1/6$ receptors. Except for the $R8$ spacing mechanism that involves long-range inhibition, all interactions are assumed to be mediated by cell-cell contacts. (b) The structure resulting from the model. The morphogenetic furrow F moves across the eye disk (the arrows show the direction of spreading). It initiates the differentiation of neural cells: a regular array of $R8$ photoreceptors develops behind it. Mystery cells M differentiate immediately anteriorly to $R8$ receptors. Later $R2$ and $R5$ are formed. The differentiation of $R3/4$ and $R1/6$ follows (these cells have not been plotted for reasons of clarity).

$$\frac{\partial h_{R8}}{\partial t} = D_{h_{R8}} \triangle h_{R8} + \rho_{h_{R8}} \left(a_{R8}^2 - h_{R8} \right) . \qquad (12b)$$

Cells begin to differentiate after they have been exposed to the morphogenetic wave. In the model, activation depends on the basic production term $\sigma_{a_{R8}} f$ in Eq. (12a). Due to the lateral inhibition *via* h_{R8} only some cells become fully activated and differentiate into $R8$ photoreceptors [Fig. 12(b)]. These cells have a precise spacing with respect to the previously activated $R8$ cells.

The diffusion range of the inhibitor h_{R8} is supposed to be of the order of several cell diameters. In the model this is the only substance with such a long diffusion range. All subsequently determined cells (M, $R2$, $R5$, etc.) differentiate under the influence of local interactions relayed by direct contact with the $R8$ cells (Banerjee and Zipursky, 1990).

3. Mystery cells M

The mystery cells M got their names because biologists were, until now, unable to assign them a role during formation of the eye; some hours after their differentiation, mystery cells die. The model suggests that M cells are used in conjunction with $R8$ neurons to induce a local polarity: like an arrow, the pair $R8$-M points to the furrow. This local memory is thought to be crucial for the correct positioning of subsequent photoreceptors, especially of $R2/5$. According to the model, the M cell acts, in conjunction with $R8$, as an initial organizer for ommatidial development by determining the primary orientation of the cell cluster and by restricting the number of cells which can choose the fate of $R2/5$. Perturbations of the furrow motion, as in White's (1961) experiment, should lead to observable alterations of the initial cluster orientation. This could be a test for the model.

The following interaction allows the activation of the M cell adjacent to the $R8$ cell:

$$\frac{\partial a_M}{\partial t} = D_{a_M} \triangle a_M + \rho_{a_M} c_M(a_{R8}) \frac{a_M^2}{h_M} - \mu_{a_M} a_M + \sigma_{a_M} f , \qquad (13a)$$

$$\frac{\partial h_M}{\partial t} = D_{h_M} \triangle h_M + \rho_{h_M} \left(a_M^2 - h_M \right) + \sigma_{h_M} . \qquad (13b)$$

The function $c_M(a_{R8})$ simulates the transmission of a signal by cell-cell contact between the putative M cell and the $R8$ neuron: this signal could, for instance, be relayed by proteins lying on the cellular membrane of $R8$ neurons. In the simulation, we chose

$$c_M(a_{R8}) = \frac{a_{R8}}{1 + \kappa_M a_{R8}^2} .$$

Due to this function, a_{R8} is required for the induction of the mystery cell, but, by reason of a disfavoring effect at very high a_{R8} concentrations, it is not the $R8$ cell itself but a neighboring cell in which a_M activation takes place. The term $\sigma_{a_M} f$, which couples the production of a_M with the furrow selects which of the $R8$ neighbors is chosen to become a mystery cell. The trail of the f wave ensures that M cells differentiate anteriorly to $R8$ neurons, so that the pair $R8$-M is like an arrow pointing to the furrow.

In the simulations, the precise positioning of M anteriorly to $R8$ is delicate; fluctuations easily disrupt this order. It could be that a similar sensitivity exists in nature. Experimentally it has been observed that cell movements play an important role in local rearrangement during genesis of the eye (Tomlinson, 1988). In this way, small errors in the precise positioning of the M cells could be corrected.

4. Recruitment of $R2/5$, $R3/4$, and $R1/6$ neurons

It is generally accepted that the subsequent differentiation of the $R2/5$ and later of the $R3/4$ and $R1/6$ photoreceptors is a consequence of cell-cell contacts. In the model, interactions with the $R8$ and M cells direct an undifferentiated cell to develop into an $R2/5$ cell. Conversely, newly formed $R2/5$ neurons inhibit their neighbors from following the same pathway. Later, other cells differentiate into $R3/4$ and $R1/6$ receptors, due to contact with $R8$ and $R2/5$ neurons. Again, $R3/4$ and $R1/6$ receptors prevent other cells in their vicinity from choosing the same fate.

These considerations suggest that equations governing the $R2/5$, $R3/4$, and $R1/6$ neuronal pathway are of the same nature as those for $R8$ and M cells. For instance, the $R2/5$ receptors are described by

$$\frac{\partial a_{R2}}{\partial t} = D_{a_{R2}} \triangle a_{R2} + \rho_{a_{R2}} c_{R2}(a_{R8}, a_M) \frac{a_{R2}^2}{h_{R2}} - \mu_{a_{R2}} a_{R2} + \sigma_{a_{R2}} , \qquad (14a)$$

$$\frac{\partial h_{R2}}{\partial t} = D_{h_{R2}} \triangle h_{R2} + \rho_{h_{R2}} \left(a_{R2}^2 - h_{R2} \right) + \sigma_{h_{R2}} . \qquad (14b)$$

Cells with a high a_{R2} concentration become $R2/5$ neurons [Fig. 12(c)]. The function c_{R2} relays a signal from $R8$ and M cells to the presumptive $R2/5$ photoreceptors:

$$c_{R2}(a_{R8}, a_M) = \frac{a_{R8}}{1 + \kappa_{R2} a_{R8}^2} \frac{a_M}{1 + \nu_{R2} a_M^2} .$$

Note that c_{R2} depends on the product of two signals. Interactions with both $R8$ and M are simultaneously required to induce the differentiation of $R2/5$ receptors.

Further differentiation of $R1/6$ and $R3/4$ photoreceptors follows the same scheme except that $c_{R2}(a_{R8}, a_M)$ is replaced by a function $c_{R3}(a_{R8}, a_{R2})$ which mimics surface contact with $R8$ and $R2/5$ neurons.

5. Abnormal eye patterns

Many mutations are known which alter the structure of the compound eye. Four of them, *rap* (Karpilov *et al.*,

1989), *Ellipse* (Baker and Rubin, 1989), *Notch* (Harris, 1991; Markopoulou and Artavanis-Tsakonas, 1991), and *scabrous* (Baker *et al.*, 1990) affect the positioning and differentiation of $R8$ cells. Based on the phenotypes of *Ellipse* and *scabrous* flies, we suggest that *Ellipse* is linked to the $R8$ activator a_{R8}, while the diffusible molecule encoded by *scabrous* may be the corresponding inhibitor h_{R8}.

In *scabrous* mutants, the $R8$ inhibition is reduced. This is modeled by *increasing* the value of $\rho_{h_{R8}}$ in Eq. (12b). For a given concentration of a_{R8}, more h_{R8} is produced and this, in turn, decreases the amount of both a_{R8} and h_{R8}; as a consequence, $R8$ cells are spaced closer together, irregularly distributed, and sometimes two $R8$ neurons are fused, as observed in *scabrous* mutants.

Notch mutants exhibit the same kind of reduced $R8$ spacing. *Notch* encodes for a transmembrane protein that is believed to be a receptor for several extracellular signals. Among them is the signal relayed by the *scabrous* protein. In this sense, the parameter $\rho_{a_{R8}}$ has to be a function of *Notch*. The model does not explicitly take this *Notch* dependance into account, but a mutation making the *Notch* protein less effective for the reception of the *scabrous* inhibition signal could decrease the value of $\rho_{a_{R8}}$ in Eq. (12a). Less activator is then produced; this decreases the h_{R8} concentration, and $R8$ cells are formed too close to each other, as observed in *Notch* mutants.

The opposite result is achieved by increasing $\rho_{a_{R8}}$. This enhances the production of a_{R8}, leading this time to an abnormally wide $R8$ spacing. It is interesting to note that the *Ellipse* mutation is believed to overactivate the gene responsible for $R8$ differentiation, in accordance with the considerations above.

It should be noted that the regulatory behaviors mentioned above are nontrivial consequences of the model: if *more* inhibitor molecules are produced per activator molecule, one achieves a *decrease* of the inhibitor concentration. This results from the nonlinear crossreaction between these two chemicals. This kind of regulatory behavior is not unique to eye development. Mutants have been found in hydra, where a decrease in the head inhibitor production rate induces, surprisingly, an increase in the head-bud spacing (Takano and Sugiyama, 1983).

Another mutation that disrupts the eye assembly is *rough* (Heberlein *et al.*, 1991). In *rough* mutants, development of ommatidia occurs normally up to $R2/5$, but $R3/4$ neurons fail to differentiate. It has been suggested (Tomlinson *et al.*, 1988; Basler *et al.*, 1990) that *rough* controls in $R2/5$ photoreceptors the signal that induces the $R3/4$ cell fate. In the model we would identify the activity of *rough* with the signal $c_{R3}(a_{R8}, a_{R2})$. Experimentally it has been observed that *rough* expression is high, first, in the morphogenetic furrow and, later, in $R2/5$ and $R3/4$ cells (Kimmel *et al.*, 1990). This corresponds to the expectation of the model.

The model is already quite complex, but it is certainly an oversimplification. For instance, the exchange of information between the cells is much more sophisticated than just a substance leaking through some holes into neighboring cells. A plausible mechanism would rather involve signaling molecules that are inserted into the membrane of one cell type and receptor molecules exposed on other cells. "Relay molecules" would then transmit the signal from the cell surface to the nucleus. There, transcriptional regulation could take place that would ultimately be responsible for the choice of the pathway. Nevertheless, this signal transduction is presumably a more or less linear chain of events, so that the approximation by a single substance exchanged by diffusion is reasonable.

Although the model seems complex, it is constructed in a straightforward way, by the successive addition of elements whose properties are well understood. These "building blocks" include wave formation, production of regular structures by simulated growth, and influence over the development of a neighboring cell. Though each single element has well defined characteristics, one learns from these models where the critical steps are. For instance, it has turned out that the generation of polarity in the periodic array of receptors is a delicate step, which is facilitated by the addition of a mystery cell.

D. Positioning mechanisms during plant growth

As a final example of a complex structure, we describe a model that allows the precise positioning of organs during the development of plants.

Plant growth occurs mainly by cell division in specialized tissues called *meristems*. The shoot apex meristem is a cone of undifferentiated cells located at the tip of stems; its cells undergo frequent mitosis. Somewhat behind the tip, the primordia are formed (Fig. 13). These will develop into leaves or flower organs. The determination of the positions at which primordia appear is believed to involve some inhibition mechanism (Schoute, 1913; Thornley, 1975; Marzec and Kappraff, 1983; Koch *et al.*, 1994). Several models have been proposed to explain the precise positioning of primordia. They are based either on the exchange of diffusible molecules (Meinhardt, 1982; Yotsumoto, 1993; Bernasconi, 1994) or on stress and pressure in the tissue (Adler, 1974, 1977a, 1977b; Green and Poethig, 1982). A pattern very similar to phyllotaxis can be generated by physical ingredients only. Under suitable conditions, mutually repelling droplets of a magnetic fluid also produce a helical arrangement (Douady and Couder, 1992).

Although a single activator-inhibitor system is able to account for the basic modes of leaf arrangement (distichous, decussate, helical) (Mitchison, 1977; Richter and Schranner, 1978; Meinhardt, 1982), it is easy to see that more complicated systems are involved. We shall discuss the necessary extensions in several steps.

Leaf initiation can take place only in a small zone at some distance from the tip of a growing shoot. Further, a signal must be available which specifies where the apical meristem is located. This suggests that at least *two* pattern-forming systems are involved. The first one determines the position of the meristem. The second gener-

ates leaves. The latter is controlled by the former: on the one hand, the meristem system represses leaf initiation at the tip but, on the other hand, it generates the precondition for this process nearby (Fig. 13). This is analogous to *Drosophila* eye development, in which a mystery cell M can emerge only in the neighborhood of a photoreceptor $R8$. Therefore leaf initiation is restricted to a narrow zone at the border of the apical meristem. A similar process takes place in the freshwater polyp *Hydra*: initiation of tentacles takes place only in a whorl around the mouth opening (Meinhardt, 1993).

However, even this more complex model is insufficient. After leaf initiation, axillary meristems are formed adjacent to the leaf primordia. They are always located on the side pointing towards the tip of the shoot. These meristematic regions do not lead immediately to cell proliferation, but they can give rise to a new shoot after the original shoot is removed. Moreover, leaves quickly attain a polarity of their own in that their upper and lower surfaces become different from each other [this process is probably induced by the neighborhood of the leaf (Sussex, 1955)]. The situation is therefore similar to that described above for eye development, since several different structures are generated in a precise periodic arrangement and with a predictable orientation.

A key for the understanding of this complex pattern is

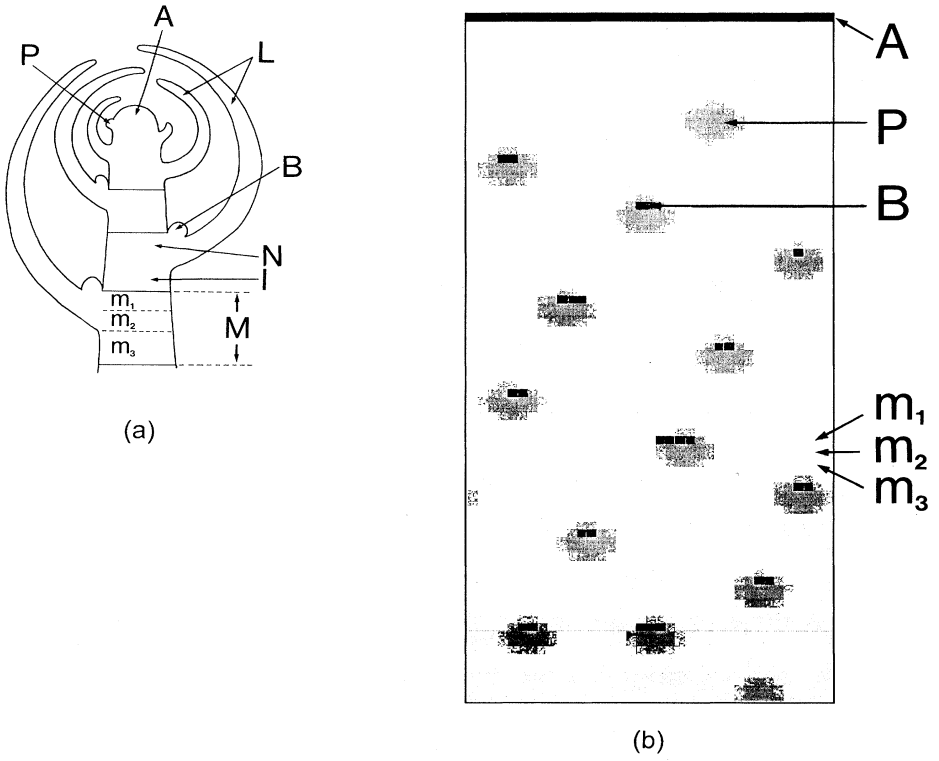

FIG. 13. The modular construction of a plant and its simulation: (a) Cross section through the growing tip of a shoot. The apical shoot meristem A is a tissue in which rapid cell division occurs. At its periphery the primordia P which will grow into leaves L appear. Axillary buds B differentiate somewhat later, in proximity to a leaf. The shoot can be regarded as a periodic repetition of an "elementary module" M formed by a node N and internode I region; every nodal-internodal segment bears a leaf L and an axillary bud B. Each module M acquires an intrinsic polarity, thanks to the iteration of at least three subunits, m_1, m_2, and m_3. (b) Simulation of plant growth. The stem of the plant is idealized as a cylinder, which is represented here unwrapped. The apical meristem A contributes to stem elongation by addition of new cells. These differentiate so as to produce the repetitive sequence $m_1\, m_2\, m_3\ m_1\, m_2\, m_3\ \ldots$ rendered here by three grey levels in the background. The $m_1 - m_2$ border acts as a positional signal for the differentiation of primordia P, identified with regions of high a_p concentration. The overlap of the primordium on the three compartments (m_1, m_2, and m_3) can be used to trigger the development of an axillary bud B ($a_M = 1$) on the m_1 segment, or of a leaf having its upper and lower face on the m_2 and m_3 segments, respectively. Note that the primordia are placed along spirals with a 2/3 phyllotaxis (the azimuthal distance between two successive primordia is approximately equal to two-thirds of the stem perimeter). Once an axillary bud is sufficiently distant from the apical meristem, it becomes active ($a_A = 1$, rendered by black squares).

its modular character (Lyndon, 1990). The elementary unit (the *module*) produced by a growing shoot consists of a node and internode segment associated with a leaf primordium and an axillary bud (Fig. 13). Leaves are always located at the top of a module, in the nodal region; axillary buds differentiate close to leaves and immediately above them. Stem elongation takes place in the internodal region (Zobel, 1989a, 1989b).

In the following, we shall propose a model based on this modular structure that accounts for the precise axial and azimuthal positioning of leaf primordia and axillary buds on the stem. The model also includes a control of meristematic activity after tip removal. Since most of the primary morphogenetic events affect only one or two surface cell layer(s), we shall idealize the plant as a hollow cylinder.

1. The apical shoot meristem

The apical meristem located at the tip of a stem represses the activity of the buds in its vicinity. The apical dominance decreases as the distance between the apex and a given bud increases with growth. This regulation is known to be mediated by phytohormones like auxins (Snow, 1940; Kühn, 1965).

We take into account two properties of the meristem. The first, modeled by a switch system a_M, tells whether a cell belongs to the apical meristem type ($a_M = 1$) or not ($a_M = 0$). A second switching system a_A controls whether the meristem is active, i.e., whether cells are undergoing frequent mitosis ($a_A = 1$) or stay in a latent state ($a_A = 0$). A further substance h_A mediates the repression of axillary bud activity. It is produced in active shoot meristems and could correspond to the phytohormone mentioned above. It must have a very long range in order to suppress meristematic activity in distant axillary buds. This long-range repression can result either from the mere diffusion of the inhibitor h_A or by some active transport mechanism of h_A in the plant. Indeed, auxin is actively transported from the shoot towards the root (Snow, 1940; Kühn, 1965). The (auxin) concentration h_A has to sink below a given level before an axillary meristem can become active, causing cell proliferation and a lateral shoot. This can occur either after substantial growth or after removal of an existing dominant tip.

The apical shoot meristem is assumed to establish a positional information system in its vicinity (Holder, 1979) to account for the observation that leaf primordia always appear at a fixed distance from the shoot apex. Such positional information is established if the active cells of the meristem produce a diffusible substance b_A. Its local concentration provides a measure for the distance from the meristem.

The previous considerations suggest the following system to describe the shoot apex meristem.

(a) Meristematic identity a_M:

$$\frac{\partial a_M}{\partial t} = \rho_M \left[\frac{a_M^2}{1+\kappa_M a_M^2} - a_M \right] + \sigma_M m_1 a_p \ . \qquad (15)$$

In a young plant, apical meristem is found only in the shoot apex, so that initially $a_M = 0$ everywhere except at the top of the stem, where $a_M = 1$. During apical growth, meristem appears in axillary buds. The term proportional to σ_M will be explained later; it corresponds to an external signal inducing the formation of an axillary bud.

(b) Activity a_A of the meristem:

$$\frac{\partial a_A}{\partial t} = \rho_A \left[\frac{a_A^2}{1+\kappa_A a_A^2} - a_A \right] + \sigma_A \frac{a_M}{1+\nu_A h_A} \ . \qquad (16)$$

Meristem activity is initiated by a signal proportional to σ_A. Due to the repression by h_A (discussed below), a bud has to reach a given distance from the apex before it can become active.

(c) Long-range inhibitor h_A of meristematic activity:

$$\frac{\partial h_A}{\partial t} = D_{h_A} \triangle h_A + \rho_{h_A} (a_A - h_A) \ . \qquad (17)$$

This is used to repress the bud activity until a given distance is achieved between the bud and the shoot apex [see the term proportional to σ_A in Eq. (16)].

(d) Positional information system b_A:

$$\frac{\partial b_A}{\partial t} = D_{b_A} \triangle b_A + \rho_{b_A} a_A - \mu_{b_A} b_A \ . \qquad (18)$$

Due to b_A, new cells begin their differentiation only at a given distance from the shoot apex, on the meristem periphery [see Eqs. (19) and (20)].

2. Building of the nodal-internodal module

Cells newly produced by mitosis in the apex "recede" from the tip of the stem. As soon as they are far enough from the meristem, they undergo differentiation. In the model, they get the information on their distance from the apical meristem from the local concentration of the substance b_A. To account for the nodal character of leaf initiation, we propose that there is a serial repetition of at least three cell states, say m_1, m_2, and m_3; the stem of a plant corresponds then to a succession of cell states like $\ldots m_1 m_2 m_3 / m_1 m_2 m_3 / m_1 \ldots$. The borders between m_1 and m_2, m_2 and m_3, m_3 and m_1 will be used in the further elaboration of the model to initiate either polar leaves or axillary bud meristems. The ordered succession of the three states m_1, m_2, and m_3 defines a *module*; the juxtaposition of m_1 and m_3 corresponds to the boundary of such a module.

The following set of equations produces, under suitable growth conditions, such a repetitive sequence [Fig. 13(b)]:

$$\frac{\partial m_i}{\partial t} = \rho_{m_i} \left[\frac{m_i^2}{h_i \left(m_{i-1}^2 + \kappa_{m_i} m_i^2 + m_{i+1}^2 \right)} - m_i \right] + \sigma_{m_i} \ , \qquad (19a)$$

$$\frac{\partial h_i}{\partial t} = D_{h_i} \triangle h_i + \rho_{h_i} \left(m_i^2 - m_{i+1} h_i \right) + \sigma_{h_i} b_A \ , \quad (19b)$$

where $i = 1,2,3$ and with the cyclic identifications $m_0 \equiv m_3$, $m_4 \equiv m_1$. Equations for (m_i, h_i) are of the activator-inhibitor type. By construction, m_i and $m_{i\pm1}$ are locally exclusive states due to the terms $m_{i\pm1}^2$ in the denominator of Eq. (19a); m_{i+1} favors the appearance of m_i in its vicinity, since it increases the removal rate of inhibitor h_i.

The set of equations given above is, of course, only an example of a system producing a repetitive sequence. What is important is that cell states locally exclude each other but activate each other over the long range (Meinhardt and Gierer, 1980). Such mechanisms have the tendency to form narrow stripes, since in this arrangement cells of a particular type are close to cells of the other types that are required for their stabilization.

It is quite amazing to observe the similarity between the above proposed model for modular growth of plants and a model for the segmentation of insects (Meinhardt, 1986, 1991). In both cases, the iteration of at least three cell states generates the periodic polar structure, and the borders between the elements are later used for accurate positioning of organs (leaves and axillary buds in plants, imaginal disks and segment borders in insects). The model for insect segmentation has found much support from observation on the molecular level. The system (19) also shares a resemblance with the *hypercycle* concept proposed for prebiotic evolution (Eigen, 1971; Eigen and Schuster, 1979): the "species" m_i are autocatalytic and compete with each other. But no species can outcompete the others, since they depend on one another for the help of m_{i+1}, which enhances the production rate of m_i.

3. Leaf primordia and axillary buds

Once a repetitive pattern $\ldots m_1 m_2 m_3 m_1 \ldots$ has been laid down it provides a convenient framework in which to initiate leaves and axillary buds along the axis. Two possibilities exist: (a) either a given structure can appear only in cells with a particular determination, for instance in m_1, or (b) the boundary between two elements, say m_1 and m_2, is required to initiate the development of that structure. These two possibilities lead to quite different predictions. Suppose that m_2 is lost due to a mutation; in the first case, this will not affect the formation of a leaf while, in the second situation, no leaves appear, due to the loss of the m_1–m_2 border. The second solution ensures, in principle, a finer positioning, since a border is always sharp. But most important, the border has a polarity. If, for instance, the signal for primordia formation can be generated only on an m_1–m_2 border, one can use the overlap of the primordium on m_1 to produce the axillary bud, while the overlap on m_2 triggers the formation of a leaf. The relative position of a bud and a leaf, the one in front of the other, is necessarily correct. Furthermore, if the signal inducing the primordium is sufficiently broad, it can also extend into the m_3 region. Let us suppose that m_2 cells can produce only the upper side and the m_3 cells only the lower side of a leaf: the polarity of the leaf is then fixed. If further proliferation is restricted to those cells close to the m_2–m_3 border, it is clear that the leaf will become flat, although the signal that induces the primordium formation has a conical shape.

To account for the features of lateral inhibition in leaf initiation, we use an activator-inhibitor system (a_p, h_p) coupled to the modular pattern in such a way that the activator peaks are initiated on m_1–m_2 borders:

$$\frac{\partial a_p}{\partial t} = D_{a_p} \triangle a_p + \rho_{a_p} h_1 m_2 \frac{a_p^2}{h_p} - \mu_{a_p} a_p + \sigma_{a_p} \ , \quad (20a)$$

$$\frac{\partial h_p}{\partial t} = D_{h_p} \triangle h_p + \rho_{h_p} a_p^2 - \left(\rho_{h_p} + \mu_{h_p} m_3 \right) h_p + \sigma_{h_p} b_A \ . \quad (20b)$$

Due to the term $\rho_{a_p} h_1 m_2$ in Eq. (20a), leaves appear close to the m_1–m_2 borders [Fig. 13(b)]. Moreover, the removal rate of h_p is increased in m_3. This accounts for the observation that the inhibition of primordia is much more effective along the shoot apex margin than axially along the stem axis (the inhibitory effect is of the order of magnitude of the apex diameter d but the axial separation of primordia is much lower than d).

Finally, each leaf induces the formation of an axillary bud in its immediate upper neighborhood, in the m_3 region [Fig. 13(b)]. Apical meristem appears in buds under the influence of the source term $\sigma_M m_1 h_p$ in Eq. (15): this term is high in m_1 subsegments only in the close vicinity of a leaf primordium.

The newly created apical meristem remains quiescent (i.e., $a_A \approx 0$) as long as the concentration of the meristematic activity inhibitor h_A remains high. It becomes active only when the inhibition sinks below a threshold [see the term proportional to σ_A in Eq. (16)]. This can occur after the shoot apex is cut (Bonner and Galston, 1952) or after substantial growth enlarges the distance between the active apical meristem and the quiescent bud.

The model is so far hypothetical. No gene system is yet known that could be responsible for the nodal-internodal structure. One reason could be that a corresponding mutation would have too severe an impact on the plant embryo, since, for instance, no leaves would be formed. Since the (at least) three elements depend on each other, the loss of one element can eliminate the others. Based on genetic observations Coen and Meyerowitz (1991) have proposed a somewhat related mechanism for the determination of the character of floral structures (sepals, petals, carpals, and stamen), but not for their positioning.

The model provides a feasible mechanism for essential elements of plant morphogenesis. It gives clues as to how polarity is established in the substructures. It predicts

that the modular nodal-internodal structure is laid down *before* initiation of leaf primordia and axillary buds. The rapidly growing data on the molecular-genetic level in plant morphogenesis will certainly provide a crucial test in the near future.

VI. CONCLUSION

We have tried to show that simple reaction-diffusion equations describing the interactions of a few chemicals provide an efficient way to understand numerous aspects of pattern formation in biology. Graded concentration profiles, periodic, and stripelike patterns can be generated out of an initially more or less homogeneous state. The regulatory properties of these mechanisms agree with many biological observations, for instance, the regeneration of a pattern with or without maintenance of polarity, insertion of new structures during growth in the largest interstices, or the generation of strictly periodic structures during marginal growth. By a hierarchical coupling of several such systems, highly complex patterns can be generated. One pattern directs a subsequent pattern and so on. Complex structures are well known from physics, for instance, in turbulence. But, in contrast, the complex patterns discussed here are highly reproducible (as well in their time development as in their spatial organization), a feature of obvious importance in biology.

Very distinct biological systems can be simulated by the assumption of basically similar mechanisms. For instance, the regular initiation of new leaves with their intrinsic polarity during plant growth and the genesis of the complex arrays of receptor cells in the developing eye of *Drosophila* are achieved by marginal growth (either real or "simulated" growth). A polarizing influence from the structure that organizes the growth, i.e., the tip of the shoot or the morphogenetic furrow, ensures the correct arrangement of the many periodically arranged substructures.

The models suggest another example of such convergence. Both the periodic pattern of insect segments and the nodal arrangement of leaves in plants are presumably achieved by the serial repetition of at least three cell states. The corresponding model for insects has been meanwhile experimentally verified (Meinhardt, 1994). All this indicates that very distantly related organisms have developed very similar mechanisms for pattern formation.

Experiments indicate that biological systems are, as the rule, much more complex than was expected from the theoretical models. There are many reasons for this. On the one hand, to bring a molecule from one cell to the next and transmit the signal to the cell's nucleus is often realized in biology by a complex chain of biochemical events, but described in the model by the mere diffusion of a substance. On the other hand, the autocatalysis of a substance may involve several steps; for instance, a small diffusible molecule may be able to activate a particular gene, which, in turn, controls the synthesis of the small molecule. The gene *goosecoid* and the small molecule *Activin* (Izpisua-Belmonte *et al.*, 1993), both involved in the generation of the primary organizing region of Amphibians, may function in this way.

Particular developmental steps have been treated as if they were isolated from the rest of the organism. In reality, they have to be integrated with many other events. The whole process has to take place at a given position within the complex organism and in a particular time window. Further, a particular developmental stage must be reached before specific subsequent steps can start. For instance, the pattern on the growing shoot must be compatible with its later transformation into a very different structure: a flower. During evolution, only modifications of existing mechanisms and the addition of new ones are allowed; a radically new construction from the beginning is impossible.

Of course, there is a strong selective pressure to make biological organisms reliable, not to make them simple. Complexity is not a problem for biological systems. For instance, a particular step can be made safe by a second parallel and independent process, as is often the case in technical processes, too (Goodwin *et al.*, 1993). That sometimes severe mutations, for instance in *Drosophila* development, produce only a mild phenotype supports such a view. If the corresponding models are then more complex too, one should not blame the theoreticians.

So far, no biological system able to generate primary pattern formation has been completely characterized at the molecular level. However, molecular biology is making tremendous progress, and we hope that the next few years will bring more evidence for the models and explain how the postulated mechanisms are actually implemented in real systems. We hope that the reader is at least convinced that the theoretical treatment of biological pattern formation is feasible and provides essential insights into the beautiful processes of life.

ACKNOWLEDGMENTS

We express our gratitude to Professor A. Gierer. Many of the basic ideas described here emerged from a fruitful collaboration with him. One of us (A.J.K.) has to thank the Max-Planck-Institut für Entwicklungsbiologie in Tübingen for its hospitality during the course of this work, and the Swiss National Fund for Scientific Research for financial support during the same period.

APPENDIX A: STABILITY ANALYSIS

This appendix is devoted to the mathematical analysis of Eqs. (1) and (3). We shall determine under which conditions the homogeneous steady state becomes unstable and leads to inhomogeneous patterns. The calculations are done explicitly for an activator-inhibitor system (1) with the restriction $\kappa_a = \sigma_h = 0$ (this greatly simplifies the calculations) and in the one-dimensional case. There

is no fundamental change if one considers the two- or three-dimensional situation, but notations become heavier. The same results can be extended to the activator-substrate model (3), in which one sets $\kappa_a = 0$.

The methods used belong to the standard tools for the study of nonlinear differential equations (Auchmuty and Nicolis, 1975; Nicolis and Prigogine, 1977; Haken, 1977).

Linearization of the dimensionless equations

It is convenient to define new time ($\bar{t}$), length ($\bar{l}$), and concentration ($\bar{a}$, $\bar{h}$) variables by use of the parameters contained in Eq. (1); written in terms of the old variables (t, l, a, and h), they read

$$\bar{t} = \mu_a t\,, \quad \bar{l} = \sqrt{(\mu_a/D_h)}\,l,$$
$$\bar{a} = \frac{\mu_a \rho_h}{\mu_h \rho_a}\,a\,, \quad \bar{h} = \frac{\mu_a^2 \rho_h}{\mu_h \rho_a^2}\,h\,.$$

Writing Eq. (1) with these new variables, we get

$$\frac{\partial \bar{a}}{\partial \bar{t}} = D\,\bar{\triangle}\bar{a} + \frac{\bar{a}^2}{\bar{h}} - \bar{a} + \sigma\,, \tag{A1a}$$
$$\frac{\partial \bar{h}}{\partial \bar{t}} = \bar{\triangle}\bar{h} + \mu\,(\bar{a}^2 - \bar{h})\,, \tag{A1b}$$

where we have introduced the abbreviations $D = D_a/D_h$, $\mu = \mu_h/\mu_a$, $\sigma = (\rho_h \sigma_a)/(\mu_h \rho_a)$, and $\bar{\triangle} = \partial^2/\partial \bar{x}^2$.

Critical length

We shall solve the system (A1) in a domain $\mathcal{D} = \{\bar{x} \mid 0 \le \bar{x} \le L\}$ and search for solutions with zero-flux boundary conditions at $\bar{x} = 0$ and $\bar{x} = L$. To simplify the notation, we shall, from now on, drop the overbars; this should not lead to any confusion.

The homogeneous steady-state solution (a_0, h_0) is found at $a_0 = 1 + \sigma$ and $h_0 = a_0^2$. Let us slightly perturb this solution: $a = a_0 + \delta a$, $h = h_0 + \delta h$ with

$$\delta a = \delta a_0\, e^{\omega t} \cos(2\pi k x), \quad \delta h = \delta h_0\, e^{\omega t} \cos(2\pi k x)\,,$$

and $|\delta a_0|$, $|\delta h_0| \ll 1$. Due to the zero-flux boundary conditions, k takes only discrete values

$$k_n = n\pi/L, \quad n = 0, 1, 2 \ldots\,. \tag{A2}$$

Each k_n is associated with a "frequency" ω_n, which can be a complex number. The functions $\omega_n(k_n)$ are found by introducing the ansatz $(a_0 + \delta a, h_0 + \delta h)$ into (A1). Retaining terms up to first order in δa and δh, we get linearized equations:

$$\mathcal{L}\begin{pmatrix} \delta a_0 \\ \delta h_0 \end{pmatrix} = 0 \quad \text{with} \quad \mathcal{L} = \begin{pmatrix} \omega_n + D\,k_n^2 + (1 - 2/a_0) & 1/a_0^2 \\ -2\mu a_0 & \omega_n + k_n^2 + \mu \end{pmatrix}.$$

The perturbation amplitudes δa_0 and δh_0 can be different from zero if and only if the discriminant of $\mathcal{L}$ is zero, $\det \mathcal{L} = 0$:

$$0 = \omega_n^2 + \alpha\,\omega_n + \beta\,, \tag{A3}$$

with

$$\alpha = (1 + D)\,k_n^2 + 1 + \mu - 2/a_0\,,$$
$$\beta = D k_n^4 + (1 + \mu D - 2/a_0)\,k_n^2 + \mu\,.$$

A fluctuation associated with the frequency ω_n grows if $\mathrm{Re}(\omega_n) > 0$. The critical length $L_c(n)$ is then defined by (Granero *et al.*, 1977)

$$\mathrm{Re}(\omega_n) = 0\,. \tag{A4}$$

If ω_n is complex, this is equivalent to $\alpha = 0$. By use of Eq. (A2), this restriction states that oscillating perturbations may be amplified in a system of length L if and only if the following inequality is verified:

$$L > L_c(n) = n\pi \left[\frac{1 + D}{2/a_0 - 1 - \mu}\right]^{1/2}.$$

Clearly, the first oscillating fluctuation that can develop in a small field is associated with $\omega(1)$, since $L_c(1) < L_c(n)$ $(n > 1)$.

Let us now consider what happens if the frequency ω_n is real. In that situation, Eq. (A4) reduces to $\beta = 0$. By use of Eq. (A2), the previous condition asserts that fluctuations associated with the frequency ω_n are amplified in a system of length L if

$$L > L_c(n) = n\pi\sqrt{2D}\left\{\left(\frac{2}{a_0} - 1 - \mu D\right) + \left[\left(\frac{2}{a_0} - 1 - \mu D\right)^2 - 4\mu D\right]^{1/2}\right\}^{-1/2}$$

Again $L_c(1) < L_c(n)$ for any $n > 1$.

In both situations, ω_n complex or real, $L > L_c(n)$ is a necessary condition for the development of an inhomogeneous state by growth of fluctuations associated with a wave number k_n. The existence of a critical length has important biological implications. A growing organism develops a nonuniform pattern only if its size becomes greater than $L_c(1)$, and the resulting structure, associated with $k_1 = \pi/L$, will be polar, having a maximum of a and h concentration on one side and a minimum on the other.

Stability diagram

Suppose now that the size L of the domain is much larger than $L_c(1)$. In this limit, we consider k as a continuous variable. Let us calculate the value $k_{\max}$ of the wave number associated with the largest positive amplification rate $\mathrm{Re}(\omega)$. In the linear approximation, $k_{\max}$ dominates the evolution of fluctuations. It is determined by the resolution of

$$\frac{\partial}{\partial k}\mathrm{Re}[\omega(k)]\bigg|_{k=k_{\max}} = 0\ , \quad \frac{\partial^2}{\partial k^2}\mathrm{Re}[\omega(k)]\bigg|_{k=k_{\max}} < 0\ , \tag{A5}$$

which state the maximality of the real part of $\omega(k_{\max})$. Fluctuations grow at this wave number if $\mathrm{Re}[\omega(k_{\max})] > 0$. We again have to make a distinction between ω as a complex or a purely real number.

If ω is complex, $\mathrm{Re}(\omega) = -\alpha/2$, and conditions (A5) show that the wave number $k_{\max} = 0$ has the largest amplification rate. It is then easily verified that, if σ is not too large ($0 \le \sigma \le 1$), $\omega(k_{\max} = 0)$ is a complex number with positive real part if the parameter μ lies in the range

$$\left[\sqrt{2/a_0} - 1\right]^2 \le \mu \le 2/a_0 - 1\ .$$

If, on the other hand, ω is real, the implicit functions theorem applied to (A3) shows that $\partial\omega/\partial k = 0$ if ω is given by

$$\omega = -\frac{\partial\beta/\partial k}{\partial\alpha/\partial k} = \frac{k_{\max}\left[2Dk_{\max}^2 + (1 + \mu D - 2/a_0)\right]}{k_{\max}(1 + D)}\ .$$

However, since the denominator of this expression is proportional to $k_{\max}$, we have to determine whether $k_{\max} = 0$ or $k_{\max} > 0$.

Let us first consider the case in which $k_{\max} > 0$. By introducing the previous solution for ω in Eq. (A3), one gets the following expression for $k_{\max}$:

$$k_{\max} = \left[\frac{2/a_0 - 1 - \mu D}{2D}\right]^{1/2}\ . \tag{A6}$$

With this value of $k_{\max}$, ω is a maximum and $\omega(k_{\max}) > 0$ if μ and D satisfy

$$\mu D < \left[\sqrt{2/a_0} - 1\right]^2\ .$$

We have, finally, to consider the situation in which ω is real and $k_{\max} = 0$. This requires $\alpha^2 - 4\beta \ge 0$. The frequency ω then has a positive maximum at $k = 0$ if μ verifies

$$0 \le \mu < \left[\sqrt{2/a_0} - 1\right]^2\ .$$

These results are summarized below and pictured in Fig. 14.

(a) If $0 < \mu < \left[\sqrt{2/a_0} - 1\right]^2$, fluctuations grow exponentially with $k_{\max} = 0$ (domain G_a in Fig. 14).

(b) If $\left[\sqrt{2/a_0} - 1\right]^2 < \mu < 2/a_0 - 1$, perturbations associated to $k_{\max} = 0$ oscillate at a fixed frequency $\mathrm{Im}(\omega)$ and grow exponentially at the time rate $\mathrm{Re}(\omega)$ (region G_b in Fig. 14).

(c) In the region $\mu \ge 2/a_0 - 1$ and $\mu D < \left(\sqrt{2/a_0} - 1\right)^2$, the uniform steady state is unstable; the system develops an inhomogeneous pattern. This corresponds to area I in Fig. 14 (this is the interesting region for morphogenesis).

(d) The homogeneous steady state is stable in the domain H defined by $\mu > 2/a_0 - 1$ and $\mu D > \left(\sqrt{2/a_0} - 1\right)^2$. Every perturbation is damped.

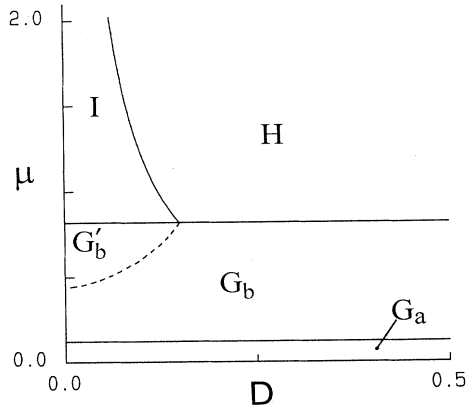

FIG. 14. Linear stability diagram for the steady-state solutions of Eqs. (A1). The behavior of fluctuations depends on the values of both D and μ. If (D, μ) belongs to the domain $G_a \cup G_b$, fluctuation amplitudes grow exponentially with (G_b) or without (G_a) oscillations. In the region I, small perturbations develop a stable inhomogeneous pattern associated with the wave number $k_{\max}$. In H, fluctuations are damped: the homogeneous steady state is stable. Taking into account nonlinear terms does not modify these conclusions, except in the region $G'_b \subset G_b$ lying near the G_b–I boundary. Two solutions compete, the first with purely real frequency and nonzero wave number, and the second with a complex frequency and $k = 0$. According to the initial value of perturbations, either a stable inhomogeneous pattern forms or an oscillating solution emerges. The exact border of G'_b depends on initial conditions, fluctuation amplitudes, etc.

The mathematical treatment supports the intuitive considerations developed in Sec. III: we find that $D = D_a/D_h \ll 1$ is needed for the development of fluctuations. The system reaches an inhomogeneous stable steady state if the removal rates of a and h verify $\mu = \mu_h/\mu_a \geq 2/a_0 - 1$.

A stability analysis has been performed with the (a, h) system (1). The activator-substrate model (3) leads to the same conclusions. Indeed, by defining appropriate variables, one can write the activator-substrate model (3), with the restriction $\kappa_a = 0$,

$$\frac{\partial a}{\partial t} = D\triangle a + sa^2 - a + \sigma$$
$$\frac{\partial s}{\partial t} = \triangle s + \mu(1 - sa^2) .$$

The homogeneous steady state is found at $a_0 = 1+\sigma$ and $s_0 = 1/a_0^2$. One introduces small perturbations according to $a = a_0 + \delta a$ and $s = s_0 - \delta s$. After linearization of the system, one is left with

$$\mathcal{L}' \begin{pmatrix} \delta a_0 \\ \delta s_0 \end{pmatrix} = 0$$

where the matrix $\mathcal{L}'$ has the same form as in the case of the activator-inhibitor system studied above. So, *mutatis mutandis*, all conclusions reached for the activator-inhibitor model apply also to the activator-substrate system.

The results given here rely on a linear analysis. Including nonlinear terms allows one, for instance, to decide the kind of bifurcation the solution undergoes when $L \approx L_c(1)$ (Haken and Olbricht, 1978) or to determine the essential features of the inhomogeneous solutions in various geometries, on a plane (Granero, Porati, and Zanacca, 1977) or on a sphere (Berding and Haken, 1982).

APPENDIX B: PARAMETER SETS

Numerical results described in this paper were obtained by implementing the models on a desktop computer. Numerical integration of the partial differential equations was performed by use of standard discretization methods. The concentration of the various chemical species a, h ... was evaluated on a two-dimensional square grid with mesh δx. Any grid point was then defined by two indexes i and j: $x_{ij} = (i\,\delta x\,, j\,\delta x)$. In two dimensions, the Laplace operator $\triangle$ applied to any function $a(x,t)$ is taken as

$$\triangle a(x_{ij},t) = \frac{a(x_{i+1\,j},t) + a(x_{i\,j+1},t) + a(x_{i-1\,j},t) + a(x_{i\,j-1},t) - 4a(x_{ij},t)}{\delta x^2} .$$

Time was also discretized, $t_k = k\,\delta t$, and the time derivative approximated by

$$\frac{\partial}{\partial t} a(x,t_k) = \frac{a(x,t_{k+1}) - a(x,t_k)}{\delta t} .$$

In all simulations, we have chosen $\delta x = \delta t = 1$. As a consequence, the border lengths of the integration domain are directly equal to the number of cells along them, and the time t is equal to the number of iteration steps. In the simulations, spatial concentration fluctuations are assumed; their order of magnitude is between 3 and 10 percent of the concentration value.

Below are listed the parameter sets used to produce the various pictures presented in the text.

Figure 1

We used Eqs. (1). Periodic boundary conditions are assumed. Initial conditions are given by the homogeneous steady state of the system. Figures 1(a) and 1(b) are calculated with the same constants but in fields of dimension 30×30 and 50×50, respectively. The parameter values used for these two pictures are listed below.

α	D_α	ρ_α	μ_α	σ_α	κ_α
a	0.005	0.01	0.01	0.0	0.0
h	0.2	0.02	0.02	–	–

Figure 1(c) is calculated in a 50×50 field with the same parameters except for $\kappa_a = 0.25$.

Figure 2

Equations used are (3). The boundary conditions are periodic and the field size is 30×30 for picture (a) and 50×50 for (b) and (c). All computations start from the homogeneous steady state. The parameter values for cases (a) and (b) are

α	D_α	ρ_α	μ_α	σ_α	κ_α
a	0.005	0.01	0.01	0.0	0.0
s	0.2	0.02	–	0.02	–

Picture (c) is calculated with the same parameters except for $\kappa_a = 0.25$. Note the correspondence with the parameters of Fig. 1.

Figure 3

The picture is computed with Eq. (5) in a one-dimensional field formed by 30 cells. Initially, $y = 0$ everywhere; the external source σ^{ext} decreases linearly, from 0.35 on the left side to 0.175 on the right side.

α	ρ_α	μ_α	κ_α
y	0.05	0.05	0.2

Figure 4

The picture is computed with Eq. (1). The boundary conditions are tight and the field grows from 21×21 to 31×31 cells. One cell line and one cell column are added at random positions after every 2000th iteration. The system is initially in its homogeneous steady state.

α	D_α	ρ_α	μ_α	σ_α	κ_α
a	0.0025	0.01	0.01	0.005	0.0
h	0.2	0.02	0.02	0.02	–

Figure 5

The picture is based on Eq. (1). The boundary conditions are tight; the field grows from 8×8 to 52×52 cells. One line and one column of cells are added at the top border and at the right-hand side after every 2000th iteration. The system starts initially out of its homogeneous steady state.

α	D_α	ρ_α	μ_α	σ_α	κ_α
a	0.006	0.01	0.01	0.001	0.0
h	0.2	0.02	0.02	0.0	–

Figure 6

The sea-urchin simulation uses Eq. (1). Boundaries are tight; the one-dimensional field grows from 5 to 50 cells, one cell being added at a random position after every 2000th iteration. The system is initially homogeneous. When the system reaches a size of 50 cells, it is cut in two parts having tight boundaries. After the cut, no further growth is assumed.

α	D_α	ρ_α	μ_α	σ_α	κ_α
a	0.005	0.0005	0.0005	0.00005	0.0
h	0.2	0.00075	0.00075	0.00025	–

Figure 7

Equations used are (7). The domain is one dimensional, initially composed of 20 cells. Zero-flux boundary conditions are assumed and the system starts from its homogeneous steady state. The field grows by addition of one cell at a random position after every 5000th iteration. When a size of 100 cells is reached, the domain is cut into two equal parts with zero-flux boundaries and the system is iterated without further growth until equilibrium is reached.

α	D_α	ρ_α	σ_α
a	0.002	2×10^{-4}	1×10^{-5}
h	0.2	2×10^{-4}	–
b	–	4×10^{-5}	–

Figure 9

The three pictures are based on Eq. (8). The field has a size of 120×65 cells in (a), and 80×80 cells in (b) and (c). For the three plots, the boundary conditions are periodic. The initial state is given by $a = 0$, $s = 3$, and $y = 0$ everywhere except on some randomly scattered point P_i where $a = 5$.

Here are the parameters used for the giraffe coat (a).

α	D_α	ρ_α	μ_α	σ_α	κ_α
a	0.015	0.025	–	–	0.1
s	0.03	0.0025	0.00075	0.00225	20.0
y	–	0.03	0.003	0.00015	22.0

To produce the leopard coat (b) we have replaced the initial conditions on s by $s = 2.5$, and on a by $a = 2$ at the positions P_i. The parameters involved are listed here.

α	D_α	ρ_α	μ_α	σ_α	κ_α
a	0.01	0.05	–	–	0.5
s	0.1	0.0035	0.003	0.0075	0.3
y	–	0.03	0.003	0.00007	22.0

The next data set produces the spots on the cheetah (d).

α	D_α	ρ_α	μ_α	σ_α	κ_α
a	0.015	0.025	–	–	0.5
s	0.1	0.0025	0.00075	0.00225	1.0
y	–	0.03	0.003	0.00015	22.0

Figure 10

Equations (9)–(10) are integrated in a field of initial dimension 50×80; one line and one column of cells are added at random positions after every 500th iteration, up to a dimension of 70×100 cells. The boundary conditions are periodic. One begins with the system in its homogeneous steady state.

α	D_α	ρ_α	σ_α	κ_α
a	0.01	0.0025	0.00025	0.1
s	0.2	0.003	0.003	–
b	0.0075	0.01875	0.00187	0.2
h	0.15	0.0375	–	–

Figure 12

The simulation is based on the set of equations (11)–(14). In this picture, the field size is of 19×24 cells. Boundaries are tight. Initially, the furrow substrate s is uniformly distributed ($s = 1$) and the furrow activator f is everywhere zero, except on four regularly spaced cells at the bottom of the field, where $f = 2$ (this initial regularity is not necessary; if $f = 2$ on the whole bottom line of the field, a regular structure emerges too, but the $R8$ cells need three or four rows to find their optimal

spacing). The other activators and inhibitors all have a very low initial concentration, say 0.01.

α	D_α	ρ_α	μ_α	σ_α	κ_α	ν_α
f	0.0025	0.1	0.011	–	0.2	–
s	–	0.04	–	–	–	–
a_{R8}	0.0025	0.04	–	0.02	–	–
h_{R8}	0.2	0.04	–	–	–	–
a_M	0.001	0.0125	0.01	0.0004	0.4	–
h_M	0.02	0.02	–	0.0002	–	–
a_{R2}	0.002	0.75	0.01	0.0001	4.0	500
h_{R2}	0.01	0.02	–	0.0001	–	–

Figure 13

The simulation is based on the set of equations (15)–(20). Zero-flux boundary conditions are imposed at the top and bottom border and periodic ones at the left-hand and right-hand sides of the field. The initial field size is 36×3. In the simulations, a_M and a_A have been rescaled so that the upper stable steady state is found at $a_M = a_A = 3$ instead of $a_M = a_A = 1$ as described in the text. Initially, meristem ($a_M = 3$) is found only on the top line of the domain; elsewhere, $a_M = 0$. The other activator and inhibitor have, respectively, 0.01 and 1.0 as initial concentrations. The domains grows by addition of one cell line after every 1500th iteration (the line is inserted two lines below the apical meristem) up to a size of 36×87 cells.

The parameters used for the simulation are listed in the following table.

α	D_α	ρ_α	μ_α	σ_α	κ_α	ν_α
a_M	–	0.01	–	0.00015	0.2222	–
a_A	–	0.01	–	0.002	0.2222	75
h_A	0.2	0.005	–	–	–	–
b_A	0.2	0.7	0.1	–	–	–
m_i	–	0.002	–	0.0004	0.1	–
h_i	0.05	0.01	–	0.011	–	–
a_p	0.004	0.005	0.01	0.001	–	–
h_p	0.2	0.01	0.02	0.1	–	–

For m_3, the value of σ_{m_3} should be replaced by 0.0002.

REFERENCES

Adler, I., 1974, "A model of contact pressure in phyllotaxis," J. Theor. Biol. **45**, 1–79.

Adler, I., 1975, "A model of space filling in phyllotaxis," J. Theor. Biol. **53**, 435–444.

Adler, I., 1977a, "The consequences of contact pressure in phyllotaxis," J. Theor. Biol. **65**, 29–77.

Adler, I., 1977b, "An application of the contact pressure model of phyllotaxis to the close packing of spheres around a cylinder in biological fine structure," J. Theor. Biol. **67**, 447–458.

Alberts, B., D. Bray, J. Lewis, M. Raff, K. Roberts, and J.D. Watson, 1989, *Molecular Biology of the Cell* (Garland, New York).

Auchmuty, J.F.G., and G. Nicolis, 1975, "Bifurcation analysis of nonlinear reaction-diffusion equations—I. Evolution equations and the steady state solutions," Bull. Math. Biol. **37**, 323–365.

Babloyantz, A., 1977, "Self-organization phenomena resulting from cell-cell contact," J. Theor. Biol. **68**, 551–561.

Baker, N.E., M. Mlodzik, and G.M. Rubin, 1990, "Spacing differentiation in the developing *Drosophila* eye: A fibrinogen-related lateral inhibitor encoded by *scabrous*," Science **250**, 1370–1377.

Baker, N.E., and G.M. Rubin, 1989, "Effect on eye development of dominant mutations in *Drosophila* homologue of the EGF receptor," Nature **340**, 150–153.

Banerjee, U., and S.L. Zipursky, 1990, "The role of cell-cell interaction in the development of the *Drosophila* visual system," Neuron **4**, 177–187.

Bard, J.B.L., 1977, "A unity underlying the different zebra striping patterns," J. Zool. Lond. **183**, 527–539.

Bard, J.B.L., 1981, "A model for generating aspects of zebra and other mammalian coat patterns," J. Theor. Biol. **93**, 363–385.

Basler, K., and E. Hafen, 1991, "Specification of cell fate in the developing eye of *Drosophila*," BioEssays **13**, 621–631.

Basler, K., D. Yen, A. Tomlinson, and E. Hafen, 1990, "Reprogramming cell fate in the Drosophila retina: transformation of *R7* cells by ectopic expression of *rough*," Genes and Development **4**, 728–739.

Bentil, D.E., and J.D. Murray, 1993, "On the mechanical theory for biological pattern formation," Physica D **63**, 161–190.

Berding, C., and H. Haken, 1982, "Pattern formation in morphogenesis," J. Math. Biol. **14**, 133–151.

Berking, S., 1981, "Zur Rolle von Modellen in der Entwicklungsbiologie," in *Sitzugsberichte der Heidelberger Akademie der Wissenschaften* (Springer-Verlag, Berlin), pp. 37–72.

Bernasconi, G.P., 1994, "Reaction-diffusion model for phyllotaxis," Physica D **68**, 90–99.

Bonner, J.S., and A.W. Galston, 1952, *Principles of Plant Physiology* (Freeman, San Francisco).

Boring, L., M. Weir, and G. Schubiger, 1993, "Egg ligation alters the bcd protein gradient and segmentation gene expression in embryos of *Drosophila*," Mech. Dev. **42**, 97–111.

Bünning, E., and H. Sagromsky, 1948, "Die Bildung des Spaltöffnungsmusters in der Blattepidermis (Mit Anmerkungen über weitere Musterbildungen)," Z. Naturforsch. **3b**, 203–216.

Castets, V., E. Dulos, J. Boissonade, and P. de Kepper, 1990, "Experimental evidence of a sustained standing Turing-type nonequilibrium chemical pattern," Phys. Rev. Lett. **64**, 2953–2956.

Chandebois, R., 1976, *Histogenesis and Morphogenesis in Planarian Regeneration*, Monographs in Developmental Biology No. 11 (Karger, Basel).

Cocho, G., R. Pérez-Pascual, J.L. Rius, and F. Soto, 1987, "Discrete systems, cell-cell interactions and color pattern of animals II. Clonal theory and cellular automata," J. Theor. Biol. **125**, 437–447.

Coen, E.S., and E.M. Meyerowitz, 1991, "The war of the whorls: genetic interactions controlling flower development," Nature **353**, 31–37.

Cooke, J., and D. Summerbell, 1980, "Cell cycle and experimental pattern duplication in the chick wing during embryonic development," Nature **287**, 697–701.

Coxeter, H.S.M., 1961, *Introduction to Geometry* (Wiley, New

York).
Crick, F., 1970, "Diffusion in embryogenesis," Nature **225**, 420–422.
Davidson, D., 1983a, "The mechanism of feather pattern development in the chick. I. The time of determination of feather position," J. Embryol. Exp. Morphol. **74**, 245–259.
Davidson, D., 1983b, "The mechanism of feather pattern development in the chick. II. Control of the sequence of pattern formation," J. Embryol. Exp. Morphol. **74**, 261–273.
de Kepper, P., V. Castets, E. Dulos, and J. Boissonade, 1991, "Turing-type chemical patterns in the chloride-iodite-malonic acid reaction," Physica D **49**, 161–169.
Diaz-Benjumea, J., M.A.F. Gonzales-Gaitan, and A. Garcia-Bellido, 1989, "Developmental genetics of the wing vein pattern of *Drosophila*," Genome **31**, 612–619.
Douady, S., and Y. Couder, 1992, "Phyllotaxis as a self-organized process," Phys. Rev. Lett. **68**, 2068–2101.
Driever, W., and Ch. Nüsslein-Volhard, 1988, "A gradient of *bicoid* protein in *Drosophila* embryos," Cell **54**, 83–93.
Eigen, M., 1971, "Selforganization of matter and the evolution of biological macromolecules," Naturwissenschaften **10**, 465–523.
Eigen, M., and P. Schuster, 1979, *The Hypercycle* (Springer, Berlin).
Ermentrout, B., J. Campbell, and G. Oster, 1986, "A model for shell patterns based on neural activity," Veliger **28**, 369–388.
Flickinger, R.A., and S.J. Coward, 1962, "The induction of cephalic differentiation in regenerating *Dugesia dorotocephala* in the presence of normal head and in unwounded tails." Dev. Biol. **5**, 179–204.
Garcia-Bellido, A., and J.F. Decelis, 1992, "Developmental genetics of the venation pattern of *Drosophila*," Annu. Rev. Genet. **26**, 277–304.
Gierer, A., 1977, "Biological features and physical concepts of pattern formation exemplified by *Hydra*," Curr. Top. Dev. Biol. **11**, 17–59.
Gierer, A., 1981, "Generation of biological patterns and form: some physical, mathematical, and logical aspects," Prog. Biophys. Mol. Biol. **37**, 1–47.
Gierer, A., and H. Meinhardt, 1972, "A theory of biological pattern formation," Kybernetik **12**, 30–39.
Goodwin, B.C., S. Kauffman, and J.D. Murray, 1993, "Is morphogenesis an intrinsically robust process?" J. Theor. Biol. **163**, 135–144.
Goss, R.J., 1974, *Regeneration. Probleme–Experimente–Ergebnisse* (Georg Thieme, Stuttgart).
Granero, M.I., A. Porati, and D. Zanacca, 1977, "A bifurcation analysis of pattern formation in a diffusion governed morphogenetic field," J. Math. Biol. **4**, 21–27.
Green, P.B., and R.S. Poethig, 1982, "Biophysics of the extension and initiation of plant organs," in *Developmental Order: Its Origins and Regulation*, edited by S. Subtelny and P.B. Green (Allan R. Liss, Inc., New York), p. 485–509.
Haken, H., 1977, *Synergetics* (Springer, Berlin).
Haken, H., and H. Olbricht, 1978, "Analytical treatment of pattern formation in the Gierer-Meinhardt model of morphogenesis," J. Math. Biol. **6**, 317–331.
Harris, W.A., 1991, "Many cell types specified by *Notch* function," Curr. Biol. **1**, 120–122.
Heberlein, U., M. Mlodzik, and G.M. Rubin, 1991, "Cell-fate determination in the developing *Drosophila* eye: role of the *rough* gene," Development **112**, 703–712.
Holder, N., 1979, "Positional information and pattern formation in plant morphogenesis and a mechanism for the involvement of plant hormones," J. Theor. Biol. **77**, 195–212.
Hörstadius, S., and A. Wolsky, 1936, "Studien über die Determination der Bilateralsymmetrie des jungen Seeigelkeimes," Roux' Arch. **135**, 69–113.
Hubel, D.H., T.N. Wiesel, and S. LeVay, 1977, "Plasticity of ocular dominance columns in monkey striate cortex," Philos. Trans. R. Soc. London, Ser. B **278**, 377–409.
Ingham, P.W., 1991, "Segment polarity genes and cell patterning within the *Drosophila* body segment," Curr. Opinions Genet. Dev. **1**, 261–267.
Ingham, P.W., and Y. Nakano, 1990, "Cell patterning and segment polarity genes in *Drosophila*," Dev. Growth Differ. **32**, 563–574.
Izpisua-Belmonte, J.C., E.M. DeRobertis, K.G. Storey, and C.D. Stern, 1993, "The homeobox gene goosecoid and the origin of organizer cells in the early chick blastoderm," Cell **74**, 645–659.
Jacobson, M., 1991, *Developmental neurobiology* (Plenum, New York).
Jaffe, L.F., 1981, "The role of ionic currents in establishing developmental pattern," Philos. Trans. R. Soc. London, Ser. B **295**, 553–566.
Karpilow, J., A. Kolodkin, T. Bork, and T. Venkatesh, 1989, "Neuronal development in the *Drosophila* compound eye: *rap* gene function is required in photoreceptor cell *R*8 for ommatidial pattern formation," Genes Dev. **3**, 1834–1844.
Kimmel, B.E., U. Heberlein, and M. Rubin, 1990, "The homeo domain protein *rough* is expressed in a subset of cells in the developing *Drosophila* eye where it can specify photoreceptor cell subtype," Genes Dev. **4**, 712–727.
Koch, A.J., J. Guerreiro, G.P. Bernasconi, and J. Sadik, 1994, "An analytic model of phyllotaxis," J. Phys. (Paris) **4**, 187–207.
Kühn, A., 1965, *Vorlesungen über Entwicklungsphysiologie* (Springer, Berlin).
Kuziora, M.A., and W. McGinnis, 1990, "Altering the regulatory targets of the deformed protein in *Drosophila* embryos by substituting the abdominal-b homeodomain," Mech. Dev. **33**, 83–94.
Lacalli, T.C., 1990, "Modeling the *Drosophila* pair-rule pattern by reaction-diffusion: Gap input and pattern control in a 4-morphogen system," J. Theor. Biol. **144**, 171–194.
Lefever, R., 1968, "Dissipative structures in chemical systems," J. Chem. Phys. **49**, 4977–4978.
Lewis, M.A., and J.D. Murray, 1992, "Analysis of dynamic and stationary pattern formation in the cell cortex," J. Math. Biol. **31**, 25–71.
Lyndon, R.F., 1990, *Plant Development. The Cellular Basis* (Unwin Hyman, London).
Lyons, M.J., and L.G. Harrison, 1992, "Stripe selection – an intrinsic property of some pattern-forming models with nonlinear dynamics," Dev. Dynamics **195**, 201–215.
Macauley-Bode, P., and H.R. Bode, 1984, "Patterning in hydra," in *Pattern Formation*, edited by G.M. Malacinski (Macmillan, London).
Markopoulou, K., and S. Artavanis-Tsakonas, 1991, "Developmental analysis of the *facets*, a group of intronic mutations at the *Notch* locus of *Drosophila melanogaster* that affect postembryonic development," J. Exp. Zool. **257**, 314–329.
Marzec, C., and J. Kappraff, 1983, "Properties of maximal spacing on a circle related to phyllotaxis and to the golden mean," J. Theor. Biol. **103**, 201–226.
Meinhardt, H., 1978, "Space-dependent cell determination

under the control of a morphogen gradient," J. Theor. Biol. **74**, 307–321.
Meinhardt, H., 1982, *Models of biological pattern formation* (Academic, London).
Meinhardt, H., 1986, "Hierarchical inductions of cell states: a model for segmentation in *Drosophila*," J. Cell Sci. Suppl. **4**, 357–381.
Meinhardt, H., 1991, "Determination borders as organizing regions in the generation of secondary embryonic fields: the initiation of legs and wings," Seminars in Dev. Biol. **2**, 129–138.
Meinhardt, H., 1993, "A model for pattern formation of hypostome, tentacles, and foot in *Hydra*: How to form structures close to each other, how to form them at a distance," Dev. Biol. **157**, 321–333.
Meinhardt, H., 1994, "Biological pattern formation: New observations provide support for theoretical predictions," BioEssays **16**, 627–632.
Meinhardt, H., and A. Gierer, 1980, "Generation and regeneration of sequences of structures during morphogenesis," J. Theor. Biol. **85**, 429–450.
Meinhardt, H., and M. Klinger, 1987, "A model for pattern formation on the shells of molluscs," J. Theor. Biol. **126**, 63–69.
Mitchison, G.J., 1977, "Phyllotaxis and the Fibonacci series," Science **19**, 270–275.
Morgan, T.H., 1904, "An attempt to analyse the phenomena of polarity in tubularia," J. Exp. Zool. **1**, 587–591.
Müller, W.A., 1990, "Ectopic head and foot formation in *Hydra*: Diacylglycerol-induced increase of positional values and assistance of the head in foot formation," Differentiation **42**, 131–143.
Murray, J.D., 1981a, "On pattern formation mechanisms for lepidopteran wing patterns and mammalian coat markings," Philos. Trans. R. Soc. London, Ser. B **295**, 473–496.
Murray, J.D., 1981b, "A pre-pattern formation mechanism for animal coat markings," J. Theor. Biol. **88**, 161–199.
Murray, J.D., 1988, "How the leopard gets its spots," Sci. Am. **258**, 80–87.
Murray, J.D., 1990, *Mathematical Biology* (Springer, Berlin).
Murray, J.D., and M.R. Myerscough, 1991, "Pigmentation pattern formation on snakes," J. Theor. Biol. **149**, 339–360.
Nicolis, G., and I. Prigogine, 1977, *Self-organization in Nonequilibrium Systems* (Wiley, New York).
Nijhout, H.F., 1978, "Wing pattern formation in Lepidoptera: a model," J. Exp. Zool. **206**, 119–136.
Nijhout, H.F., 1980, "Pattern formation in lepidopteran wings: determination of an eyespot," Dev. Biol. **80**, 267–274.
Ouyang, Q., J. Boissonade, J.C. Roux, and P. de Kepper, 1989, "Sustained reaction-diffusion structures in an open reactor," Phys. Lett. A **134**, 282–286.
Ready, D.F., 1989, "A multifaceted approach to neural development," Trends Neurosci. (TINS) **12**, 102–110.
Ready, D.F., T.E. Hanson, and S. Benzer, 1976, "Development of the *Drosophila* retina, a neurocrystalline lattice," Dev. Biol. **53**, 217–240.
Richter, P.H., and R. Schranner, 1978, "Leaf arrangement. geometry, morphogenesis, and classification," Naturwissenschaften **65**, 319–327.
Rothen, F., and A.J. Koch, 1989a, "Phyllotaxis, or the properties of spiral lattices. I. Shape invariance under compression," J. Phys. (Paris) **50**, 633–657.
Rothen, F., and A.J. Koch, 1989b, "Phyllotaxis or the properties of spiral lattices. II. Packing of circles along logarithmic spirals," J. Phys. (Paris) **50**, 1603–1621.
Schoute, J.C., 1913, "Beiträge zur Blattstellung," Recueil des Travaux Botanique Néerlandais **10**, 153–325.
Segel, L.A., and J.L. Jackson, 1972, "Dissipative structure: an explanation and an ecological example," J. Theor. Biol. **37**, 545–549.
Séguy, E., 1973, "L'aile des insectes," in *Traité de Zoologie*, edited by P.-P. Grassé (Masson et Cie, Paris), Vol. VIII, Part 1, pp. 595–702.
Serfling, E., 1989, "Autoregulation,. a common property of eucariotic transcription factors?" Trend Genetics **5**, 131–133.
Shimizu, H., Y. Sawada, and T. Sugiyama, 1993, "Minimum tissue size required for *hydra* regeneration," Dev. Biol. **155**, 287–296.
Slack, J.M.W., 1987, "Morphogenetic gradients — past and present," Trends Biochem. Sci. (TIBS) **12**, 200–204.
Snow, R., 1940, "A hormone for correlative inhibition," New Phytologist **39**, 190–199.
Steindler, D.A., A. Faissner, and M. Schachner, 1989, "Brain "cordones": Transient boundaries of glia and adhesion molecules that define developing functional units," Comments Dev. NeuroBiol. **1**, 29–60.
Stern, C.D., 1986, "Do ionic currents play a role in the control of development?" BioEssays **4**, 180–184.
Summerbell, D., 1974, "Interaction between the proximodistal and anteroposterior coordinates of positional value during the specification of positional information in the early development of the chick limb-bud," J. Embryol. Exp. Morphol. **32**, 227–237.
Sussex, I.M., 1955, "Morphogenesis in *Solanum tuberosum* L.: Experimental investigation of leaf dorsiventrality and orientation in the juvenile shoot," Phytomorphology **5**, 286–300.
Takano, J., and T. Sugiyama, 1983, "Genetic analysis of developmental mechanisms in hydra. VIII. head-activation and head-inhibition potentials of a slow-budding strain (L4)," J. Embryol. Exp. Morphol. **78**, 141–168.
Thaller, C., and G. Eichele, 1987, "Identification and spatial distribution of retinoids in the developing chick limb bud," Nature **327**, 525–629.
Thaller, C., and G. Eichele, 1988, "Characterization of retinoid metabolism in the developing chick limb bud," Development **103**, 473–484.
Thornley, J.H.M., 1975, "Phyllotaxis. I. A mechanistic model," Ann. Bot. Fenn. **39**, 491–507.
Tickle, C., 1981, "The number of polarizing region cells required to specify additional digits in the developing chick wing," Nature **289**, 295–298.
Tomlinson, A., 1988, "Cellular interactions in the developing *Drosophila* eye," Development **104**, 183–193.
Tomlinson, A., B.E. Kimmel, and G.M. Rubin, 1988, "*rough*, a *Drosophila* homeobox gene required in photoreceptors *R*2 and *R*5 for inductive interactions in the developing eye," Cell **55**, 771–784.
Turing, A.M., 1952, "The chemical basis of morphogenesis," Philos. Trans. R. Soc. London, Ser. B **237**, 37–72.
Vardasca, J., A. de Wit, G. Dewel, and P. Borckmans, 1992, "Reentrant hexagonal Turing structures," Phys. Lett. A **168**, 194–198.
White, R.H., 1961, "Analysis of the development of the compound eye in the mosquito, *Aedes aegypti*," J. Exp. Zool. **148**, 223–237.
Wigglesworth, V.B., 1940, "Local and general factors in the

development of pattern in *Rhodnius prolixus* (hemiptera)," J. Exp. Biol. **17**, 180–200.

Wilby, O.K., and G. Webster, 1970, "Experimental studies on axial polarity in hydra," J. Embryol. Exp. Morphol. **24**, 595–613.

Wolpert, L., 1969, "Positional information and the spatial pattern of cellular differentiation," J. Theor. Biol. **25**, 1–47.

Wolpert, L., J. Hicklin, and A. Hornbruch, 1971, "Positional information and pattern regulation in regeneration of hydra," Symp. Soc. Exp. Biol. **25**, 391–415.

Wolpert, L., and A. Hornbruch, 1981, "Positional signalling along the anteroposterior axis of the chick wing. The effect of multiple polarizing region grafts," J. Embryol. Exp. Morphol. **63**, 145–159.

Yotsumoto, A., 1993, "A diffusion model for phyllotaxis," J. Theor. Biol. **162**, 131–151.

Zobel, A.M., 1989a, "Origins of nodes and internodes in plant shoots. I. Transverse zonation of apical parts of the shoot," Ann. Bot. **63**, 201–208.

Zobel, A.M., 1989b, "Origins of nodes and internodes in plant shoots. II. Models of node and internode origin from one layer of cells," Ann. Bot. **63**, 209–220.

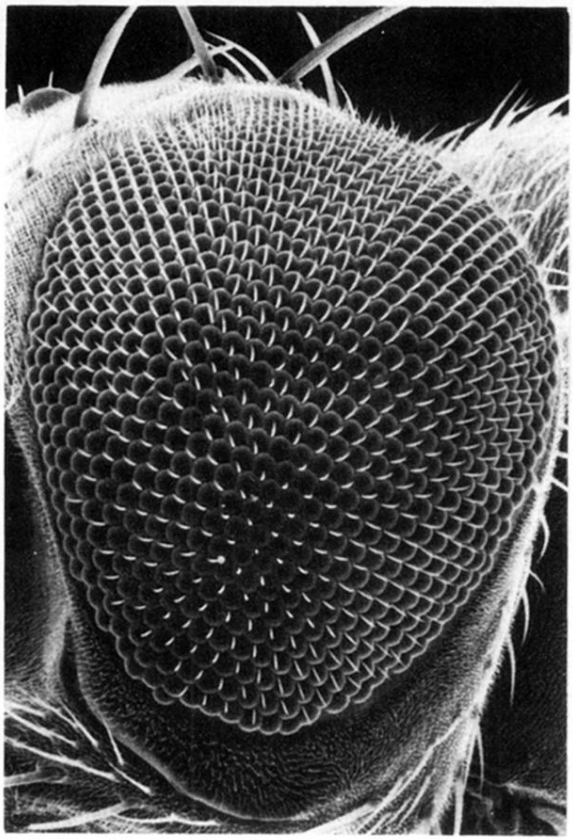

(a)

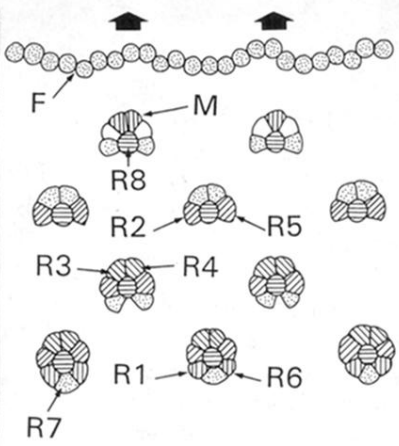

(b)

FIG. 11. Overall structure of the *Drosophila* eye and its genesis: (a) Scanning electron micrograph of the eye of a *Drosophila* fly showing the regular array of ommatidia (photograph kindly provided by J. Berger). (b) Pattern formation of the *Drosophila* eye. A morphogenetic furrow F sweeps anteriorly across the eye-antennal imaginal disk (the arrows show the direction of propagation). Behind the furrow, ommatidial assembly begins with the differentiation of regularly spaced $R8$ photoreceptors, each one associated with one or two mystery cells M. Later $R2$ and $R5$ neurons are recruited, followed by the formation of $R3$, $R4$, $R1$, $R6$, and, finally, $R7$ receptors; M cells are meanwhile eliminated by selective cell death. After formation of all photoreceptors, 12 other cells are added in every ommatidium (cone, pigment, and bristle cells). Dots indicate differentiating cells while hatches show differently differentiated cells.

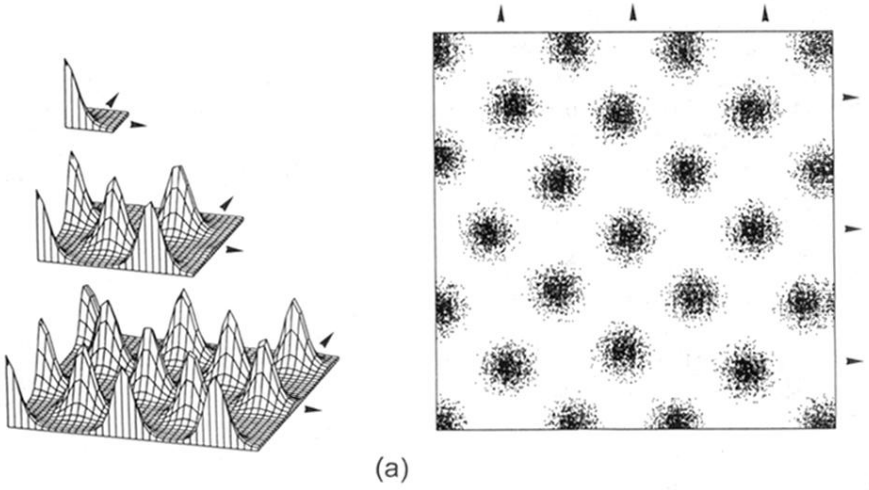

(a)

(b)

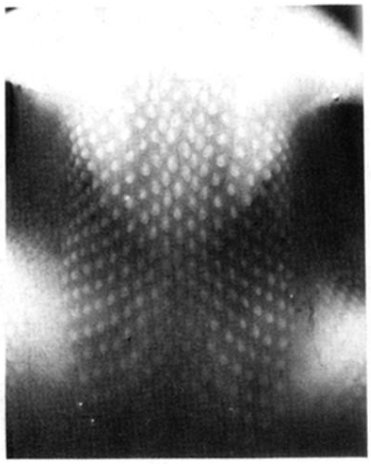

(c)

FIG. 5. Generation of periodic structures during marginal growth: (a) In this simulation, the domain enlarges by addition of new cells at the upper and left borders; a periodic structure emerges. Plotted is the activator of an (a, h) model. (b) The regular spacing of thorns on this cactus is achieved by apical growth (see also Sec. V). The thorns are arranged along helices that wrap around the stem. (c) Feather primordia are regularly spaced on the back of a chicken. To position them accurately, the chicken "simulates" growth by use of a determination wave that starts from the dorsal midline and spreads on both sides: only cells reached by the wave can initiate the development of primordia. The wave motion simulates growth by enlarging the region competent for feather production (photograph by courtesy of Dr. H. Ichijo).

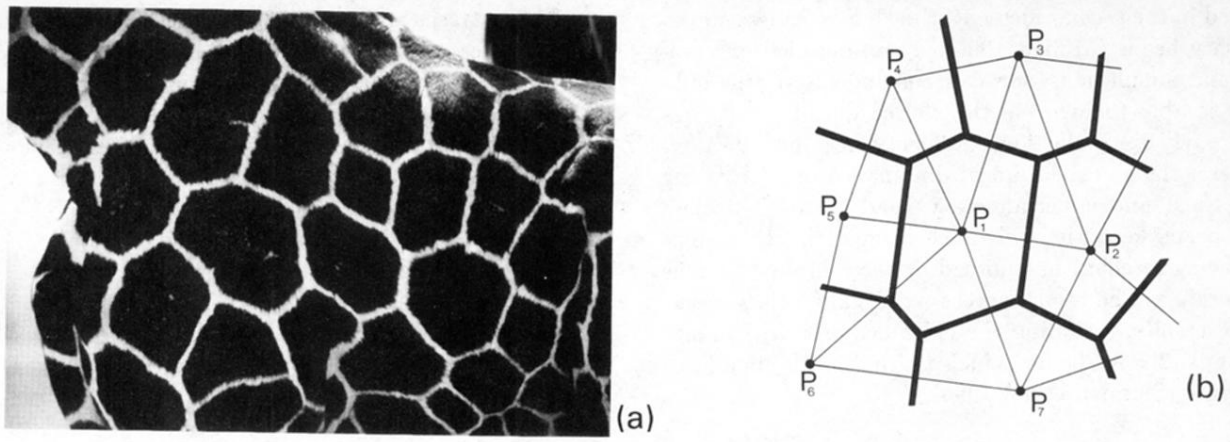

FIG. 8. Analogy of the giraffe pattern with Dirichlet domains. (a) Side of a giraffe (*Giraffa camelopardalis reticulata*). The pattern is formed by convex polygons separated by thin lines (photograph kindly provided by O. Berger). The formal resemblance with Dirichlet domains is suggestive. (b) Construction and definition of Dirichlet domains. Given a set $\{P_1, \ldots, P_n\}$ of points belonging to a surface $\mathcal{S}$, one draws the perpendicular bisectors between neighboring points. The convex envelop surrounding a center P_i delimits its associated Dirichlet domain $\mathcal{D}_i$. By construction, $\mathcal{D}_i$ contains all the points of the surface $\mathcal{S}$ nearer to P_i than to any other P_j $(j \neq i)$.